NUREG/CR-0500
TREE-1270
for U.S. Nuclear Regulatory Commission

AN ASSESSMENT OF FUEL MELTING, RADIAL EXTRUSION, AND CLADDING THERMAL FAILURE DURING A POWER-COOLING-MISMATCH EVENT IN LIGHT WATER REACTORS

MOHAMED S. EL-GENK

May 1979

EG&G Idaho, Inc.

IDAHO NATIONAL ENGINEERING LABORATORY

DEPARTMENT OF ENERGY

IDAHO OPERATIONS OFFICE UNDER CONTRACT EY-76-C-07-1570

Available from
National Technical Information Service
Springfield, Virginia 22161
Price: Printed Copy A04; Microfiche $3.00

The price of this document for requesters outside the North American continent can be obtained from the National Technical Information Service.

NUREG/CR-0500
TREE-1270
R3

AN ASSESSMENT OF FUEL MELTING, RADIAL EXTRUSION, AND CLADDING THERMAL FAILURE DURING A POWER-COOLING-MISMATCH EVENT IN LIGHT WATER REACTORS

Mohamed S. El-Genk

EG&G Idaho, Inc.
Idaho Falls, Idaho 83401

Published May 1979

PREPARED FOR THE
U. S. NUCLEAR REGULATORY COMMISSION
AND THE U. S. DEPARTMENT OF ENERGY
IDAHO OPERATIONS OFFICE
UNDER CONTRACT NO. EY-76-C-07-1570
NRC FIN NO. A6046

ACKNOWLEDGMENTS

The author thanks Dr. P. Hofmann (Kernforschungszentrum Karlsruhe, West Germany), Dr. M. Epstein (Argonne National Laboratory), and Dr. S. J. Dagbjartsson for the helpful discussion on the general aspects of the analysis, and Dr. D. W. Croucher for his comments and review of this report.

ABSTRACT

The thermal behavior of the fuel and the cladding during off-normal operating conditions in light water reactors (LWRs) are of great importance to reactor safety evaluation. In the present work, fuel conditions during a hypothesized power-cooling-mismatch (PCM) accident in LWRs are characterized with regard to pellet cracking and fuel melting. Melting of UO_2 fuel at the center of the pellet during a PCM accident in which film boiling is present at the cladding surface, is assessed by employing a simplified steady state analysis. The induced pressure at the center of the pellet due to fuel melting, fission gas release, and UO_2 fuel vapor may force molten fuel to penetrate through radially open cracks in the outer unmelted portion of the pellet and relocate in the fuel-cladding gap. The contact of molten fuel with zircaloy cladding, which is at high temperatures during film boiling, may initiate cladding melting at its inside surface and eventually result in a thermal failure of the cladding.

An analytical model is developed to study the transient freezing of a superheated liquid penetrating an initially empty crack, maintained at a constant, subfreezing temperature. The analysis is presented in a dimensionless form, demonstrating the effect of the governing parameters; namely, the driving pressure, crack shape, crack length, liquid flow conditions, thermophysical properties, and the temperature of the liquid and the crack walls. The calculational results are applied to the radial extrusion of molten UO_2 fuel, observed in some in-pile tests in which PCM conditions were simulated.

Conditions for potential melting of the zircaloy cladding upon being contacted by the extruded molten fuel are investigated analytically. The analytical predictions are consistent with the experimental results from PCM in-pile tests.

SUMMARY

The behavior of light water reactor fuel rods during off-normal operating conditions is being studied as part of the Thermal Fuels Behavior Program conducted by EG&G Idaho, Inc., for the Nuclear Regulatory Commission. Irradiation effects (IE) and power-cooling-mismatch (PCM) in-pile tests have been performed in the Power Burst Facility (PBF) at the Idaho National Engineering Laboratory to provide data on the behavior of irradiated and unirradiated pressurized water reactor fuel rods under various PCM and power ramp conditions. Extensive central fuel melting, up to 80% of the pellet radius, and radial extrusion of molten fuel into the fuel-cladding gap were observed in some of those tests. Contact of extruded molten fuel with zircaloy cladding which is at high temperature during film boiling may induce cladding failure due to melting, because of the great difference between the melting point of the fuel and that of the cladding.

The primary objectives of the present work are (a) to assess fuel conditions during a hypothesized PCM event with regard to pellet cracking and fuel melting at the center of the pellet, (b) to develop an analytical model for the transient freezing of a superheated liquid penetrating an initially empty crack and apply the results to the radial extrusion of molten fuel observed in some of the PCM in-pile tests, and (c) to analytically investigate the conditions for melting of zircaloy cladding upon being contacted by the extruded molten fuel and compare the results with in-pile experiments in which a PCM event was simulated.

Fuel pellet cracking usually occurs during normal reactor operation. The parabolic temperature distribution developed in the fuel rods during normal operation produces a thermoelastic stress which exceeds the UO_2 fuel tensile strength at the periphery of the pellet, thereby forming cracks along radial and horizontal planes. Crack size and population in the outer region of the pellet depend on the reactor power and the irradiation history of the fuel. If a PCM event occurs, film boiling may be produced at the outer surface of the cladding, causing fuel and cladding temperatures to increase rapidly. Fuel melting may initiate at the pellet centerline, propagating radially outward. The radius of the melting zone and the temperature of molten fuel at the pellet center depend on reactor power and pellet surface temperature. Volumetric expansion at the pellet center caused by UO_2 fuel melting, fission gas release, and fuel vapor pressure increase the openings of the cracks at the periphery of the pellet and may force molten fuel to extrude radially through these open cracks into the fuel-cladding gap.

A physical model is developed to study the transient freezing of a superheated liquid as it penetrates a short, initially empty crack. The behavior of the deposited frozen crust on the crack walls and the liquid penetration length into the crack, as functions of time, are studied analytically and demonstrated graphically in a dimensionless form, illustrating the effect of the governing parameters; namely, the driving pressure, crack shape and dimensions, liquid flow conditions, and thermophysical properties and temperatures of the liquid and the crack walls. The application of the model to molten fuel extrusion in PBF in-pile tests indicates that successive solidification of extruded molten fuel on crack walls could easily block the crack, causing most of the molten fuel to remain at the pellet center. However, if the amount of molten fuel extruded into the fuel-cladding gap prior to crack blockage is sufficient to establish physical contact with the cladding, the molten fuel freezes onto the inside surface of the cladding and may initiate simultaneous melting of the cladding at the common interface. Conditions for potential melting of the cladding upon being contacted by the extruded molten fuel are assessed using an exact analytical model. The model studies the transient freezing of a stagnant, superheated liquid on a semi-infinite wall which undergoes simultaneous melting.

Comparison of the analytical calculations for molten fuel extrusion with the results from in-pile experiments indicates that the molten fuel extruded into the fuel-cladding gap in some of those tests was slightly superheated, so that the frozen crust at the crack walls continued to grow until it reached a steady state thickness of less than half the crack opening. This freezing partially blocked the crack, while molten fuel continued to flow from the center of the pellet into the fuel-cladding gap. In other cases in which crack blockage occurred before molten fuel was able to completely penetrate the crack length, the extruded fuel

was at its fusion temperature and the driving pressure was small. This driving pressure could have been induced by the capillary forces (∿0.004 MPa) because of the small width of the cracks (∿75 μm). Since the maximum fuel superheat in those tests is not expected to have exceeded several hundred degrees, the pressure contribution due to fuel vapor at the pellet center is calculated to be higher than the capillary forces (for example, 0.1 MPa when fuel superheating is 500 K). The axial movement of molten fuel, however, could have been a cause for the reduced pressure at the pellet center.

The analytical results indicate that the onset of melting of zircaloy cladding upon being contacted by molten fuel depends on fuel and cladding temperatures and on the metallurgical composition at the inner surface of the cladding (that is, alpha-zircaloy or ZrO_2) at the time of contact. Thermal failure of oxygen-stabilized alpha-zircaloy cladding due to melting upon being contacted by molten fuel at the fusion temperature would occur if the cladding temperature during film boiling was ≥1660 K. However, the existence of a ZrO_2 layer at the inner surface of the cladding would delay the onset of melting at the inside surface of the cladding (the ZrO_2) up to an initial cladding temperature of ≈2640 K. At such elevated temperatures, the middle layers of the cladding (which may be either oxygen-stabilized alpha-zircaloy or beta-zircaloy, or both) would already be in a molten state. If the extruded fuel was superheated rather than at its fusion temperature, zircaloy cladding melting would occur at lower initial cladding temperatures. In the PCM in-pile tests considered in this report, cladding melting was not observed. The absence of cladding melting in those tests is explained by the fact that the temperatures of the extruded fuel and the zircaloy cladding were below the level required to initiate cladding melting upon being contacted by molten fuel.

NOMENCLATURE

a	half width of the crack (m)
A	dimensionless pressure (Table II)
B	time-dependent coefficient [Equation (11)]
C_1, C_2	constants [Equation (20)]
C_p	specific heat (J/kg·K)
d	molten fuel-solid fuel average density ratio [Equation (A-2)]
E	time-dependent coefficient [Equation (29)]
f	friction factor [Equations (18) and (19)]
F	time-dependent coefficient [Equation (29)]
h	convective coefficient of heat transfer ($W/m^2 \cdot K$)
h_f	latent heat of fusion of molten UO_2 (J/kg)
k	thermal conductivity (W/m·K)
K	pressure loss coefficient [Equation (15)]
K_c	entrance pressure loss coefficient [Equation (16)]
K_f	pressure loss coefficient due to friction [Equation (18)]
L	total length of the crack (m)
m	mass (kg)
P	pressure (MPa)
P_o	pressure at the liquid free surface outside the crack entrance (MPa) [Equation (17)]
P_g	pressure in the crack at the liquid penetration front (MPa) [Equation (17)]
Pe	Peclet number (Re·Pr) [Equation (30)]
Pr	Prandtl number
q'	linear power (kW/m)
q'''	volumetric power (kW/m^3)

Re	Reynolds number
R_c	central void radius (m)
R_m	molten fuel radius (m)
R_s	fuel pellet radius (m)
SN	Stefan number for freezing [Table II and Equation (33)]
t	time (s)
T_J	temperature of molten fuel (K)
T_c	temperature at the face of the fuel pellet (K)
T_f	fusion temperature (K)
T_m	temperature in molten fuel (K)
T_{mp}	melting point of the cladding (K)
T_o	initial temperature in the solid cladding (K)
T_s	temperature in the solid fuel (K)
T_w	temperature in the crack wall (K)
v	liquid bulk average velocity (m/s)
Y	half width of the flow area in the crack (m)
z	axial coordinate (m)
w	wetting coefficient [Equation (35)]
W	volume (m^3)

Greek Letters

α	kinematic viscosity-thermal diffusivity ratio (Table II)
α_{sf}	thermal diffusivity in the solid fuel (m^2/s)
α_{mf}	thermal diffusivity in the molten fuel (m^2/s)
β	dimensionless flow area (Table II)
β_{sm}	solid fuel-molten fuel thermal diffusivity ratio [Equation (33)]
γ	crack shape factor (Table II) or surface tension (MPa/m) [Equation (34)]

δ	frozen crust thickness (m)
Δ	dimensionless frozen crust thickness
θ	contact angle (Figure 23)
θ_1	dimensionless temperature of molten fuel [Equation (33)]
θ_2	dimensionless melting temperature of zircaloy cladding [Equation (33)]
λ	freezing constant [Equations (13) and (33)]
ν	kinematic viscosity (m^2/s)
σ	molten cladding-solid fuel thermal ratio [Equation (33)]
ℓ	liquid penetration length in the crack (m)
ϕ	dimensionless penetration length of the liquid (Table II)
$\phi_{blockage}$	dimensionless penetration length of the liquid when complete blockage of the crack occurs
ψ	dimensionless velocity (Table II)
ε	density ratio (Table II)
ρ	density (kg/m^3)
τ	dimensionless time (Table II)

Subscripts

e	at crack exit
i	at crack ertrance
LV	liquid-gas interface
m	molten
mc	molten cladding
mf	molten fuel
sc	solid cladding
sm	solidified molten
s,sf	solid fuel

SL	solid-liquid interface
SV	solid-gas interface
T	total
w	wall
z	at axial position z
ℓ	at the liquid penetration front

CONTENTS

FIGURES

TABLES

AN ASSESSMENT OF FUEL MELTING, RADIAL EXTRUSION, AND CLADDING THERMAL FAILURE DURING A POWER-COOLING-MISMATCH EVENT IN LIGHT WATER REACTORS

I. INTRODUCTION

The primary safety consideration in the design of nuclear reactors is to ensure that no conceivable accident, whether initiated by a failure of the reactor system or by incorrect operation, will lead to a dangerous release of radiation to the environment. A number of hypothesized accidents must be considered in the design and licensing of light water reactors (LWRs). The extreme examples have traditionally been known as loss-of-coolant accidents (LOCAs), in which a part or all the coolant would be lost from the active core, and reactivity initiated accidents (RIAs), in which there would be a rapid increase in power due to, for example, control rod ejection (pressurized water reactor) or control rod dropout (boiling water reactor). Between these two extremes, various off-normal power or cooling conditions, generally termed power-cooling-mismatch (PCM) accidents, may be induced, in which the coolant would usually fail to successfully remove the generated heat within the core.

During a PCM accident, film boiling may occur at the cladding surface and cause the fuel and cladding temperatures to increase rapidly, perhaps producing embrittlement of the zircaloy cladding[1-4] due to oxidation. Fuel melting may initiate at the center of the pellet and propagate radially outward. Such molten fuel may extrude through radially open cracks in the outer, unmelted portion of the pellet and relocate in the fuel cladding gap. Contact of extruded molten fuel with the cladding, which is at high temperature during film boiling, may initiate cladding melting.

Extensive central melting of the fuel, up to 80% of the pellet radius, was observed in the in-pile tests in which PCM conditions were simulated[5-8]. (These tests were performed for the Nuclear Regulatory Commission in the Power Burst Facility at the Idaho National Engineering Laboratory as part of the Thermal Fuels Behavior Program conducted by EG&G Idaho, Inc.) Although radial extrusion of molten fuel into the fuel-cladding gap was evident in some of these tests, the zircaloy cladding exhibited no evidence of melting at its inner surface upon being contacted by the extruded molten fuel. The absence of cladding melting may have been due to one or more of the following causes: (a) the amount of extruded molten fuel may have been insufficient to produce complete physical contact with the zircaloy cladding (such insufficient extrusion occurs when radial cracks in the pellet become blocked early because of the solidification of the extruded fuel on crack walls); (b) a zirconium dioxide layer (ZrO_2 melting point = 2950 K) may have formed at the inner surface of the cladding due to a sufficient oxygen potential in the fuel; or (c) at the time of contact, the temperature of either the zircaloy cladding or the molten fuel, or both, may have been sufficiently low, such that the temperature at the common interface did not reach or exceed the melting point of the cladding. Adequate understanding of the scenario of a PCM accident in LWRs is necessary to assess fuel melting, molten fuel radial extrusion and refreezing phenomena, and to investigate the conditions necessary for a potential thermal failure of the cladding due to melting upon being contacted by molten fuel.

The purposes of the present work were (a) to assess fuel conditions during a hypothesized PCM event with regard to cracking and melting at the center of the pellet, (b) to develop an analytical model for the transient freezing of a superheated liquid penetrating an initially empty crack and apply the results to the radial extrusion of molten fuel observed in some of the PCM in-pile tests, and (c) to analytically investigate the conditions for melting of zircaloy cladding upon being contacted by the extruded molten fuel and compare the results with in-pile experiments in which a PCM event was simulated.

Section II characterizes fuel conditions during a PCM event with regard to pellet cracking, fuel melting, and pressure sources that might contribute to molten fuel extrusion from the melting zone at the pellet center through radially open cracks into the fuel-cladding gap. In Section III, an analytical study is presented for the transient freezing of a superheated liquid as it penetrates an initially empty crack, the walls of which were maintained at a constant subfreezing temperature. The calculations are applied to molten UO_2 radial extrusion observed in PCM in-pile experiments. In Section IV, the initial conditions that might produce freezing of extruded molten fuel and initiate simultaneous melting of solid zircaloy cladding are studied analytically. The analytical predictions are compared with the applicable results from in-pile experiments. Conclusions are presented in Section V; supporting analyses are contained in the appendices.

II. FUEL CONDITIONS DURING A POWER-COOLING-MISMATCH EVENT

As a result of normal power operation, fuel pellets are cracked and partially relocated within the rod. Depending on the fuel temperature and irradiation history, sintering of the UO_2 will occur during operation to partially heal the cracks. If a power-cooling-mismatch event was to occur, film boiling could be initiated at the outer surface of the cladding. The resultant reduction in the heat transfer coefficient at the cladding outside surface would produce a rapid temperature rise in the cladding and the fuel. Fuel melting may initiate at the pellet centerline and propagate radially outward. The potential extrusion of this molten fuel into the fuel-cladding gap and subsequent contact with the zircaloy cladding depends, in general, on the shape, size, and number of cracks in the unmelted portion of the fuel pellet, the amount of superheat in the molten fuel, the temperature in the crack walls, and the driving forces that cause the extrusion.

Fuel conditions during a PCM event with regard to cracking, central melting, and the driving forces producing molten fuel extrusion are reviewed in the following subsections. Examples of molten fuel extrusion that occurred during in-pile simulations of PCM events in pressurized water reactors are also presented.

1. FUEL CRACKING

Polycrystalline ceramic UO_2 is a hard and brittle material which has essentially no capacity for plastic deformation below ≈1470 K. At sufficiently high temperatures (generally above 1670 K), however, UO_2 exhibits a measurable amount of plastic deformation before fracture occurs. Deformation and fracture behavior of stoichiometric UO_2 have been studied[9-11]. Three regions of temperatures, shown in Figure 1, were identified as brittle, semibrittle, and plastic. As demonstrated in Figure 2, the brittle region occupies the range from room temperature to a transition temperature at which a measurable plastic deformation prior to ductile fracture first occurs. This transition temperature is called the ductile-brittle transition or nil ductility temperature, which was found[10] to be equal to 1470 K when the applied strain was increased at a rate of 0.1 h^{-1} and the grain size in the specimen was ~15 μm. At higher strain rates, however, the transition from brittle to ductile behavior would occur at higher temperatures, independent of the grain size. The temperature range of 1470 to 1670 K prescribes the semibrittle region, in which the transition from completely brittle to purely ductile behavior occurs. In the plastic core at temperatures above 1670 K, appreciable plastic deformation occurs before ductile failure. Stoichiometric UO_2 flows very easily under low stress and therefore does not crack, but, like a liquid, it cannot sustain a stress field other than pure compression.

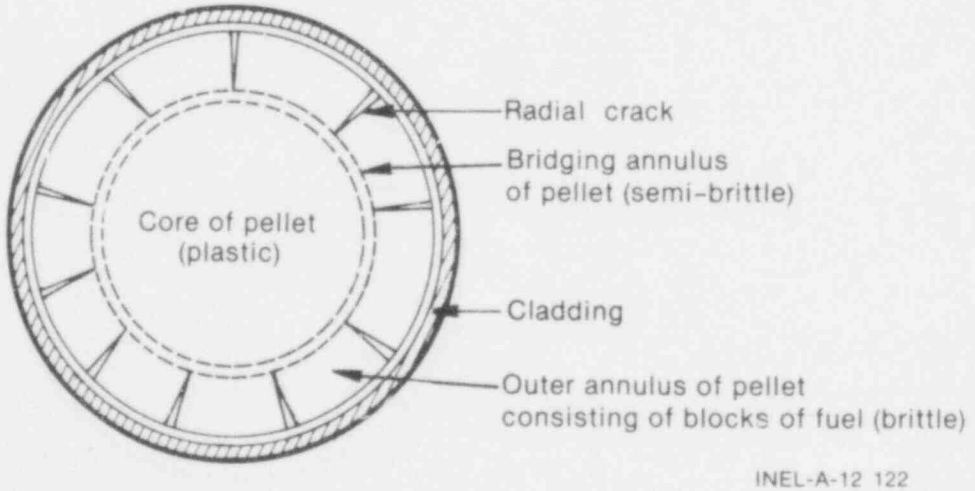

Fig. 1 Radial crack distribution in a UO_2 fuel pellet.

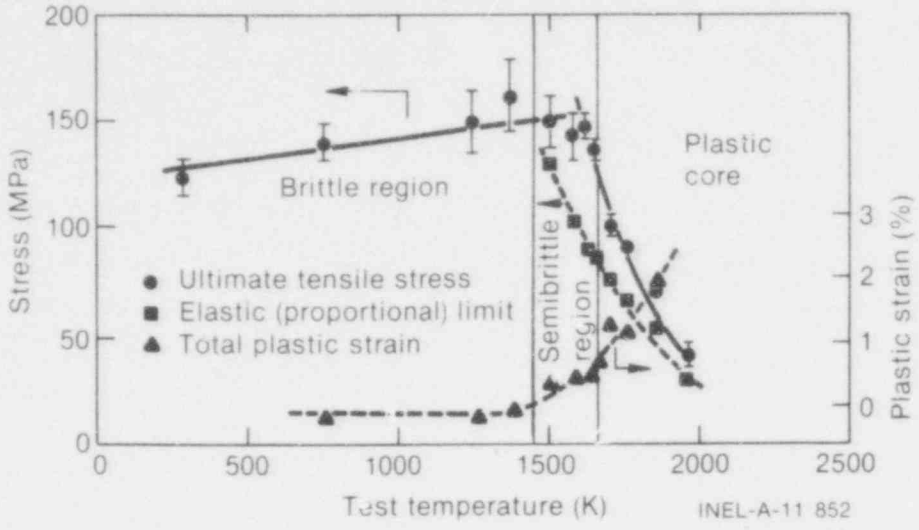

Fig. 2 Fracture and flow characteristics of UO_2 as functions of temperature. (The strain rate was ~0.1 h^{-1} and the grain size of the specimen was ~15 μm.)

During normal operation the thermoelastic stress components induced by the parabolic temperature gradient in the fuel rod exceed the tensile fracture strength of the fuel in the outer portion of the pellets. A network of cracks oriented along either radial or horizontal planes is therefore developed in the outer region of the UO_2 fuel pellets, where the fuel temperature is less than 1670 K. Figure 3[12] illustrates a theoretical shape of a fuel pellet in which UO_2 fuel expands under the effect of thermoelastic stresses. As indicated,

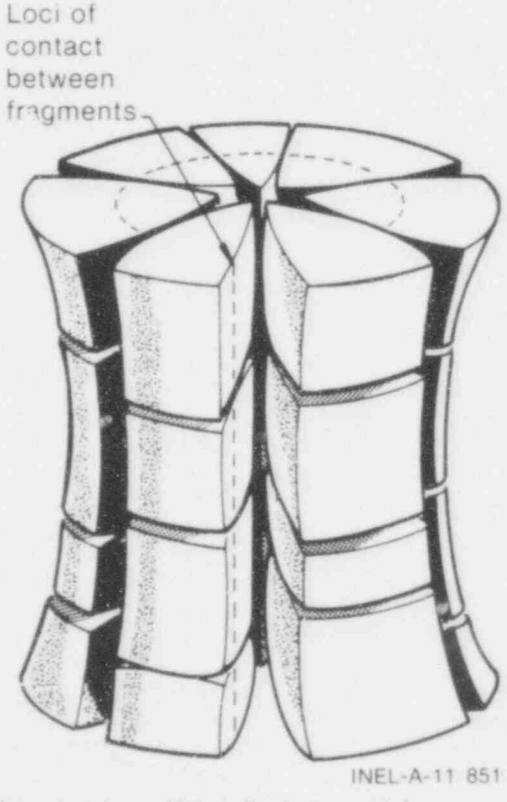

Fig. 3 Theoretical shape of UO_2 pellet during normal reactor operation.

the radial expansion of the fuel pellet is larger at the ends than at the center section due to the thermoelastic effect in a finite cylinder[13], in which the induced stresses are respectively compressive and tensile in the inner and outer radial portions of the pellet. At the end faces, however, both the tangential and radial stresses are everywhere tensile, producing a greater radial expansion at the ends. This type of deformation has not been observed in tubing containing either powder compacted or single, full length rods of UO_2. It occurs only when the fuel is in the form of cylindrical pellets, whether solid or hollow.

The width and population of cracks in a UO_2 pellet during reactor operation depends to a great extent on the operating power and the irradiation history of the fuel. Some typical crack patterns for irradiated fuel, observed in postirradiation examinations of instrumented fuel assemblies irradiated in the Halden Boiling Water Reactor (HBWR) at Halden, Norway, are shown in Figure 4[14]. At low power, fuel pellets

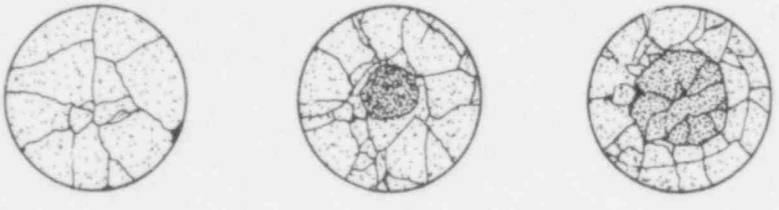

Fig. 4 Some typical crack patterns in irradiated UO_2 fuel pellets (3000 MWd/kg U).

have shown some irregular circumferential cracks. At high powers, the outermost circumferential cracks tend to occur around the brittle-to-ductile transition boundary, which is between 1470 to 1670 K. Different patterns of fuel cracking for unirradiated, BWR-6 fuel tested under steady state conditions in the Power Burst Facility are shown in Figure 5[15]. Operation at low local power generated a major crack varying from 65 to 260 μm in width. The cracks produced at higher local power were more numerous and of smaller width. Irregular circumferential cracks were also generated; the outermost ones are thought to be located near the region of the nil ductility temperature of UO_2 (~1470 K).

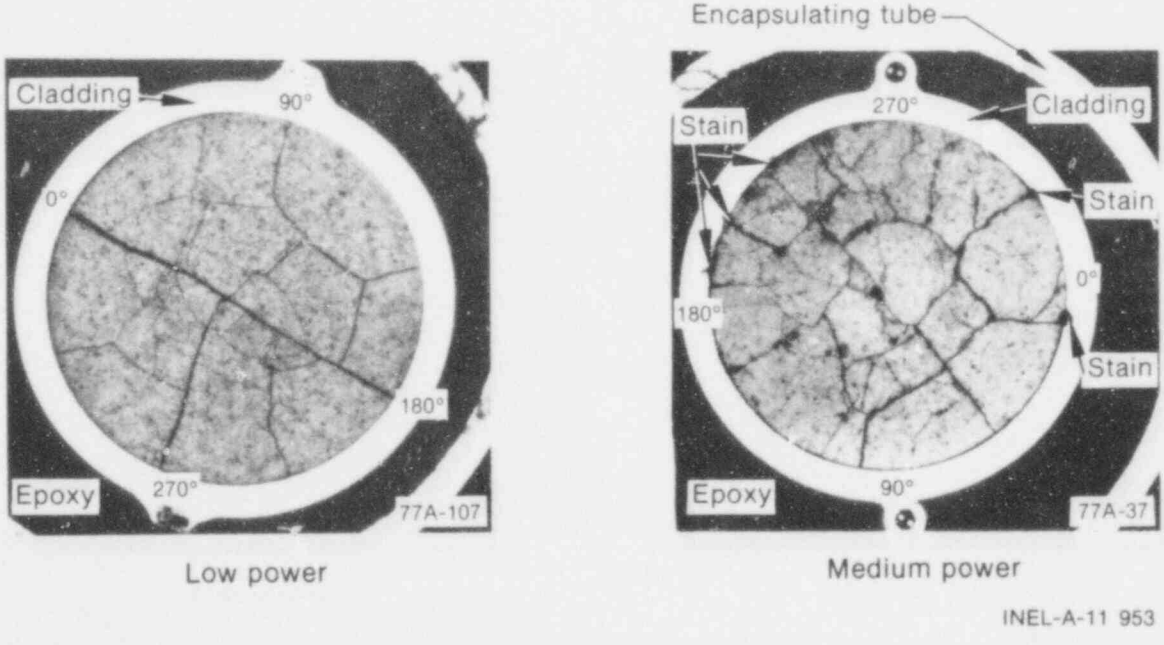

Fig. 5 Different patterns of fuel pellet cracking for unirradiated, nominal design, BWR-6 fuel.

Figure 6 presents a summary of the general trend of cracking in UO_2 pellet fuel, 12 to 14 mm in diameter, which was examined after irradiation in the HBWR. A plot of the number of main radial cracks (cracks less than 3 to 5 degrees apart are counted as one main crack) versus the temperature gradient at the periphery of the fuel pellet is shown in the figure. The experimental results from instrumented irradiated fuel assemblies and from Reference 10 are compared in Figure 6(a) with theoretical predictions based on finite element calculations introduced in Reference 14. Figure 6(b) demonstrates the change in the total number of radial cracks in terms of the temperature gradient at the periphery of the pellet. As indicated, increasing the temperature gradient increases the number of total cracks relative to the number of main cracks.

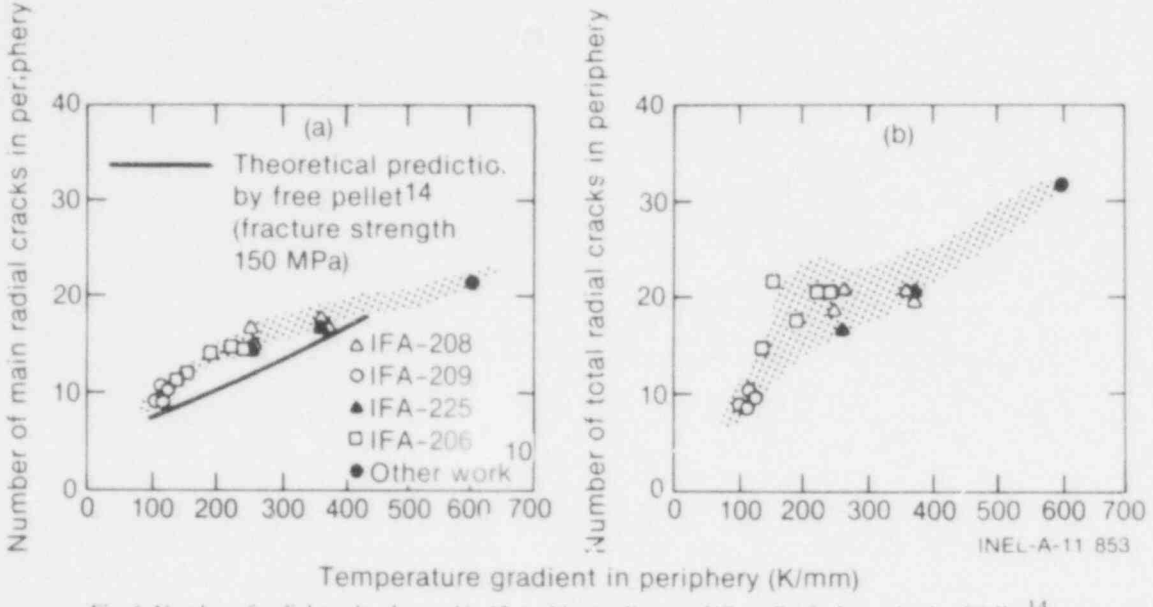

Fig. 6 Number of radial cracks observed in 12- to 14-mm-diameter UO_2 pellet fuel examined at Kjeller[14].

This evidence illustrates that cracking of the fuel pellets occurs during normal operation. The size, number, and orientation of the cracks vary with fuel irradiation history and the reactor operating power. Many of the cracks located in the outer portion of the pellet may provide paths by which molten fuel from the pellet centerline could relocate into the fuel-cladding gap.

2. CENTRAL FUEL MELTING

In this section, a simplified steady state calculation is presented to assess the radius of fuel melting at the center of the pellet in the film boiling zone, for rods operating during a hypothesized PCM accident, as a function of the local linear operating power and the temperature at the pellet surface. The corresponding degree of superheating in the molten UO_2 fuel is also predicted. A detailed derivation of the governing equations in both the molten and solid regions of a cylindrical fuel pellet is presented in Appendix A.

The local linear power to onset melting at the center of a fuel rod can be obtained from the relation

$$\int_{T_c}^{T_f} k_s \, dT_s = \frac{q'}{4\pi} \, . \qquad (1)$$

Increasing the operating power or reducing the coolant rate to initiate film boiling at the cladding surface could induce fuel melting at the center of the pellets. In this case, the temperature integral in the outer, solid region of the fuel pellet (assuming no central void) is given [Equation (A-11)] as

$$\int_{T_c}^{T_f} k_s \, dT =$$

$$\frac{\dot{q}}{4\pi} \left[\frac{1 - (R_m/R_s)^2 + 2 (R_m/R_s)^2 \ln(R_m/R_s) - 2 d (R_m/R_s)^2 \ln(R_m/R_s)}{1 - (R_m/R_s)^2 (1 - d)} \right] \tag{2}$$

and in the central molten fuel zone [Equation (A-10)] as

$$\int_{T_f}^{T_b} k_m \, dT = \frac{\dot{q}}{4\pi} \left[\frac{(R_m/R_s)^2 d}{1 - (R_m/R_s)^2 (1 - d)} \right]. \tag{3}$$

Through use of the data given in Table I for the thermophysical properties of UO_2 fuel, Equations (2) and (3) are solved simultaneously (numerically) for both the degree of superheating in the molten fuel, $(T_b - T_f)$, and the molten fuel percentage of the initial radius of the pellet, $(R_m/R_s)\%$, as functions of the linear operating power, $\dot{q}$, and the temperature at the pellet surface, T_c. The calculational results are demonstrated graphically in Figures 7 and 8.

As shown in Figure 7, increasing the temperature at the surface of the fuel pellet, either due to poor gap conductance or to film boiling at the outside surface of the cladding, initiates central fuel melting at progressively lower operating powers. The radius of the melting zone at the center of the pellet and the corresponding superheating in the melted fuel are strongly influenced by the pellet surface temperature and the linear operating power, as can be seen in Figure 8. Increasing either the operating power or the pellet surface temperature increases the melting radius and the degree of superheating in the melted fuel. Figure 8 provides sufficient information to predict the molten fuel radius, the superheat in the melted fuel, and the vapor pressure of molten fuel at the center of the pellet, if both the linear operating power and the fuel pellet surface temperature are known.

TABLE I

THERMOPHYSICAL PROPERTIES OF UO_2 FUEL

Property	Phase	Value	Temperature Range (K)	Reference
Melting point (K)		3100	--	16
Heat of fusion (J/kg)		2.74×10^5	1350	16
Density (kg/m^3)	Solid[a]	$\frac{11.004463 \times 10^{-3}}{[1 + 9 \times 10^{-6} T + 6 \times 10^{-9} T^2 + 3 \times 10^{-12} T^3]}$	273 to 3073	17
	Liquid[b]	$\frac{8.74 \times 10^{-3}}{[1 + 1.05 \times 10^{-4} (T - 2865^b)]}$	3138 ≤ T	18
Specific heat (constant pressure) (J/kg·K)	Solid	$(134 + 1.8 T - 3.1 \times 10^{-5} T^2)$	1300 to 2300	19
	Liquid	5×10^2	3170 to 3520	20

TABLE 1 (continued)

Property	Phase	Value	Temperature Range (K)	Reference
Thermal conductivity (W/m·K)	Solid[a]	$(40.4 \times 10^{2})/(464 + T) + 1.216 \times 10^{-2} \exp(1.867 \times 10^{-3} T)$	2731 to 1923	16
	Solid[a]	$1.91 + 1.216 \times 10^{-2} \exp(1.867 \times 10^{-3} T)$	1923 to 3113	16
	Liquid	2.5	3170 to 3470	20

a. The temperature in this expression is in ^{o}C.

b. The melting point of UO_2 is assumed to be 3138 K in this expression instead of 3100 K.

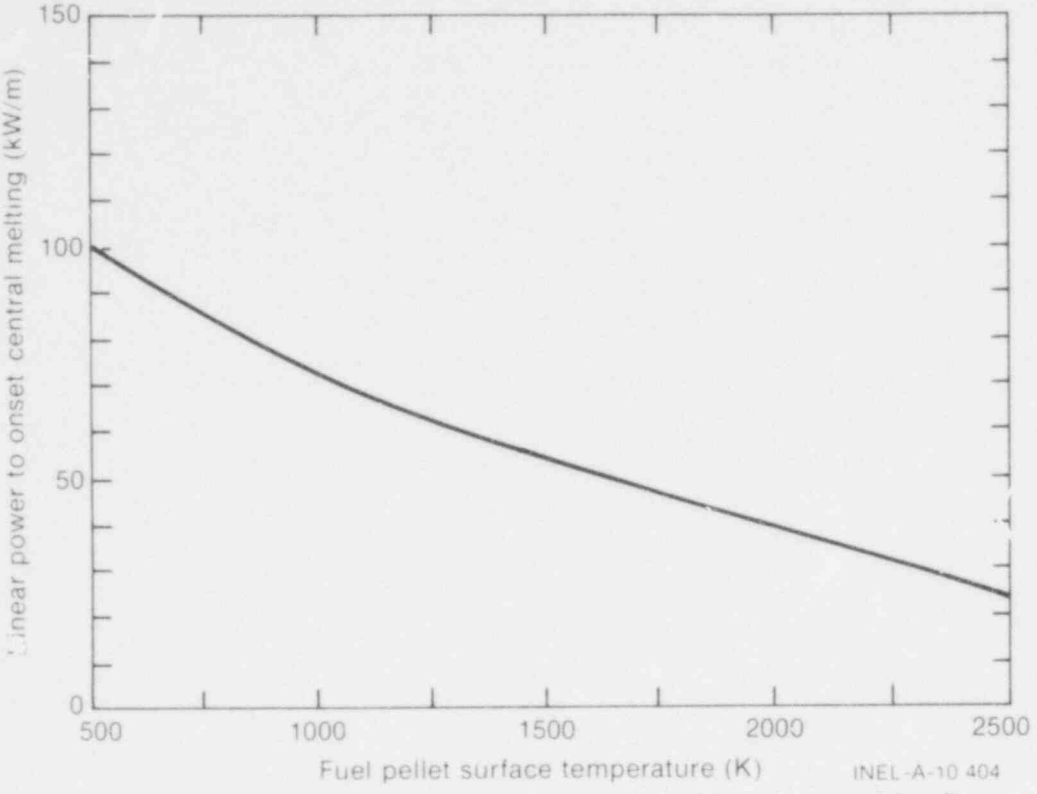

Fig. 7 Effect of fuel pellet surface temperature on the onset of fuel melting at the center of the pellet.

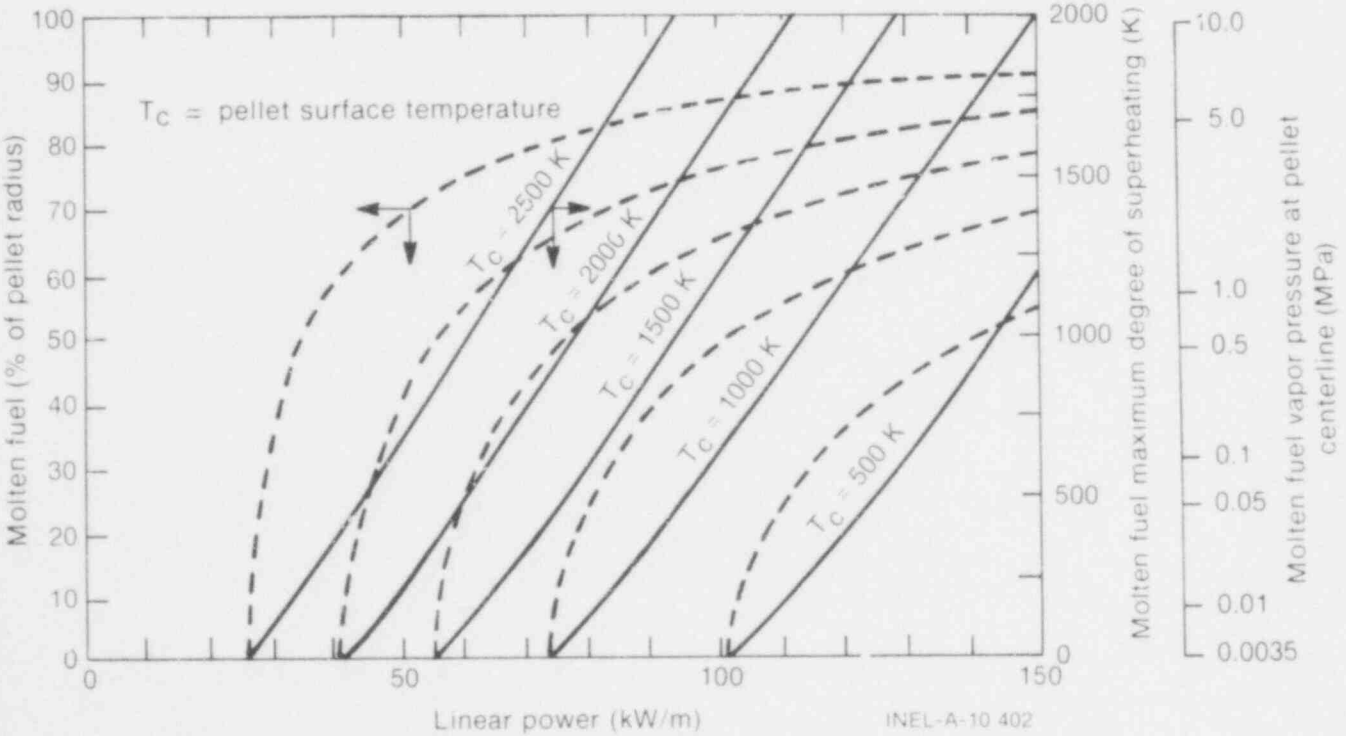

Fig. 8 Percentage of central fuel melting and molten fuel superheating as functions of linear operating power and temperature at the pellet surface.

3. EXAMPLES OF CENTRAL FUEL MELTING AND MOLTEN FUEL RADIAL EXTRUSION

Power-cooling-mismatch tests[5-8] have been performed in the Power Burst Facility to provide data on the behavior of irradiated and unirradiated pressurized water reactor fuel rods under various simulated PCM conditions. Examples of central fuel melting and radial extrusion of molten fuel observed in some of those tests are presented in this section.

As a result of the PCM conditions simulated during these in-pile tests, film boiling was established at the surface of the cladding. In the film boiling zone, extensive central fuel melting of up to 80% of the pellet radius and extrusion of molten fuel into the fuel-cladding gap were observed in those rods in which the peak operating power was ~65 kW/m. The parabolic temperature profile in the fuel pellet causes gaseous pores and fission gases within the central molten zone to migrate up the thermal gradient to form a void at the center of the pellet. The radius of this void depends on the linear operating power, the duration of film boiling, the radius of the central melting zone, and the irradiation history of the fuel. Figure 9 illustrates the fuel microstructure and central melting typically observed in irradiated and unirradiated fuel during PCM in-pile tests. Figures 10 and 11 show once-molten fuel extrusion from the pellet center through radially open cracks within the film boiling zone in irradiated rods, in which the local operating power was about 55 kW/m. Figure 12 shows another example of molten fuel extrusion into the pellet dishes observed in one of these rods.

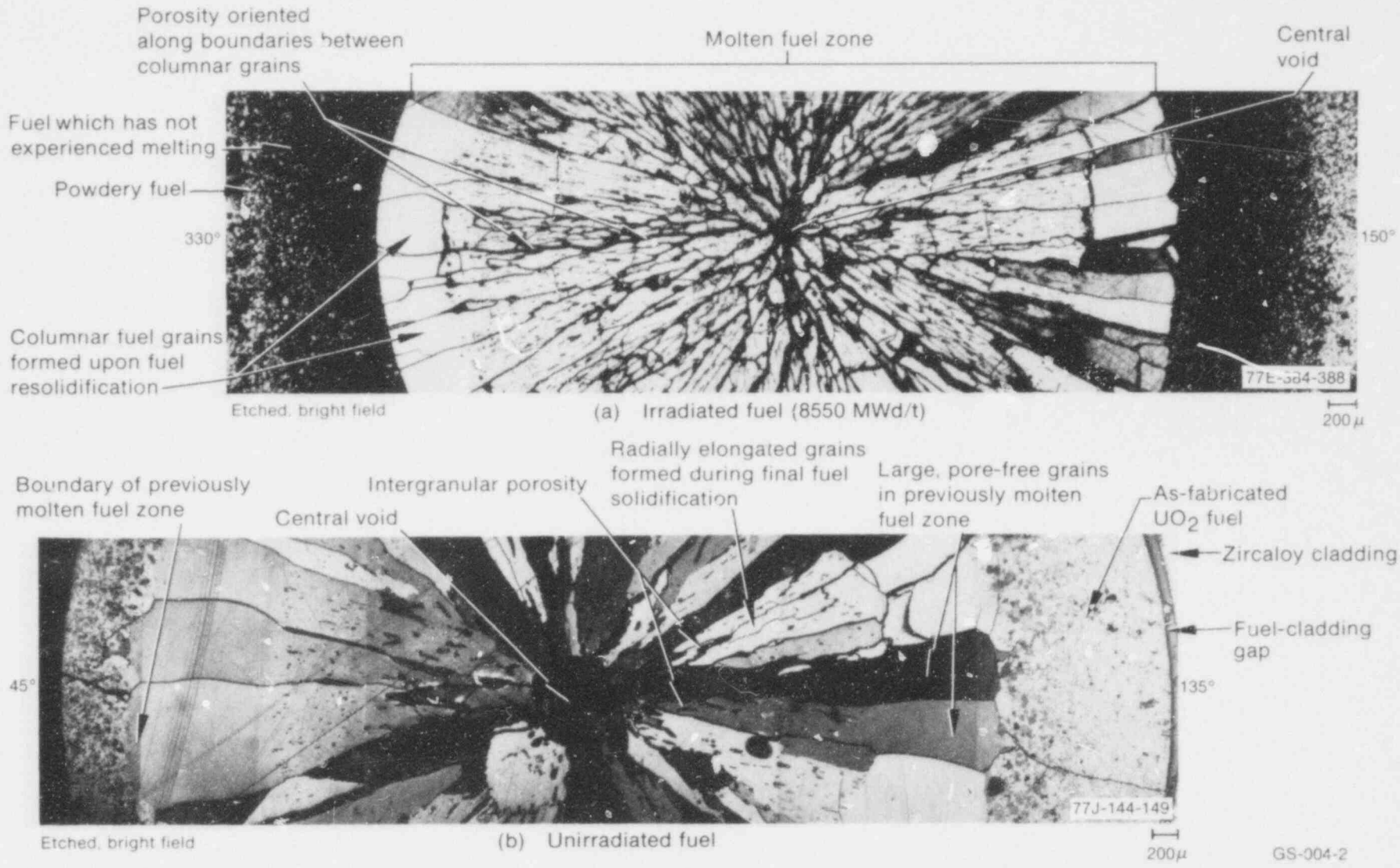

Fig. 9 Fuel microstructure and central melting in the film boiling zone observed in PCM in-pile tests.

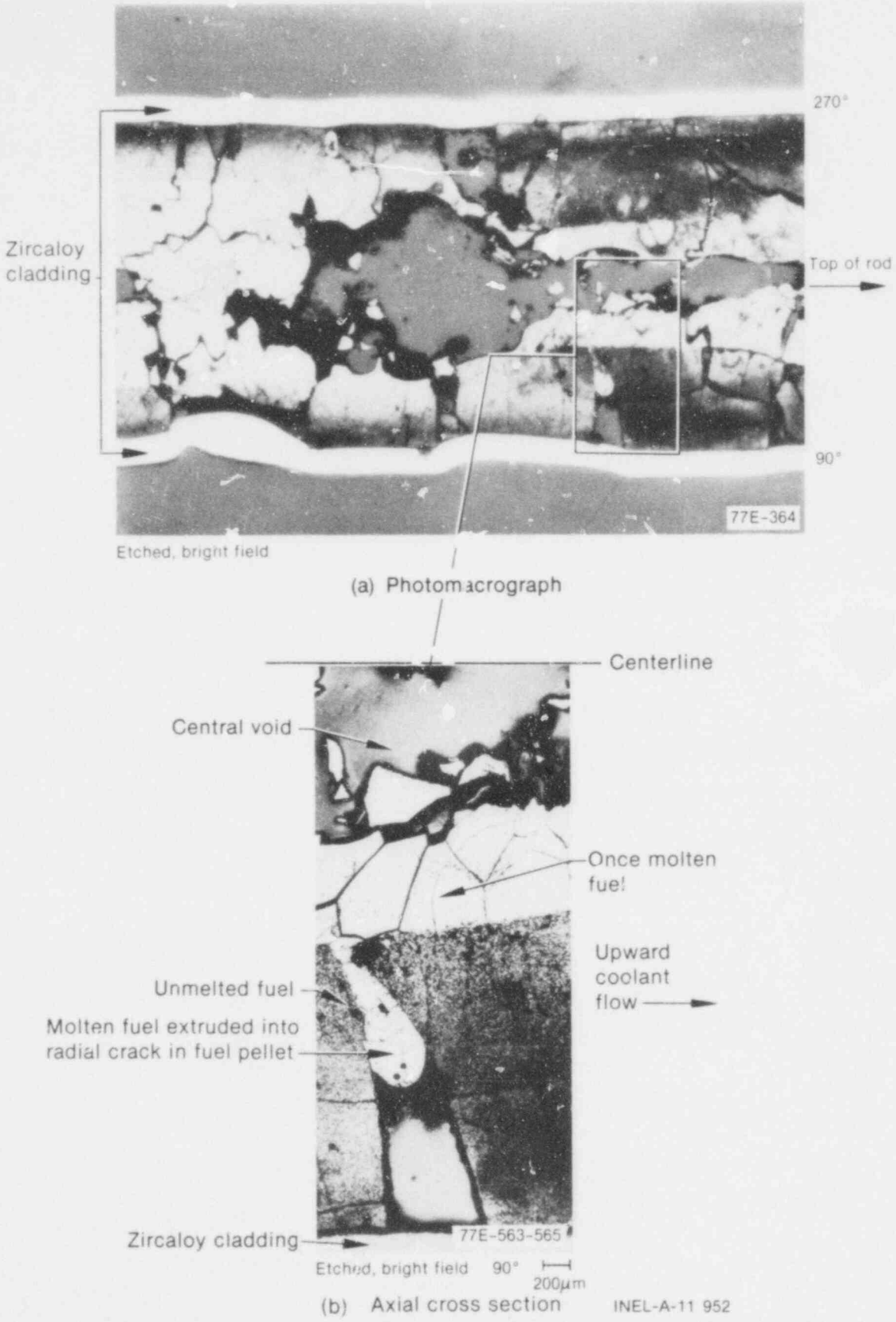

Fig. 10 Molten fuel extrusion through a radial crack in the outer, unmelted portion of the pellet observed during PCM in-pile test[6].

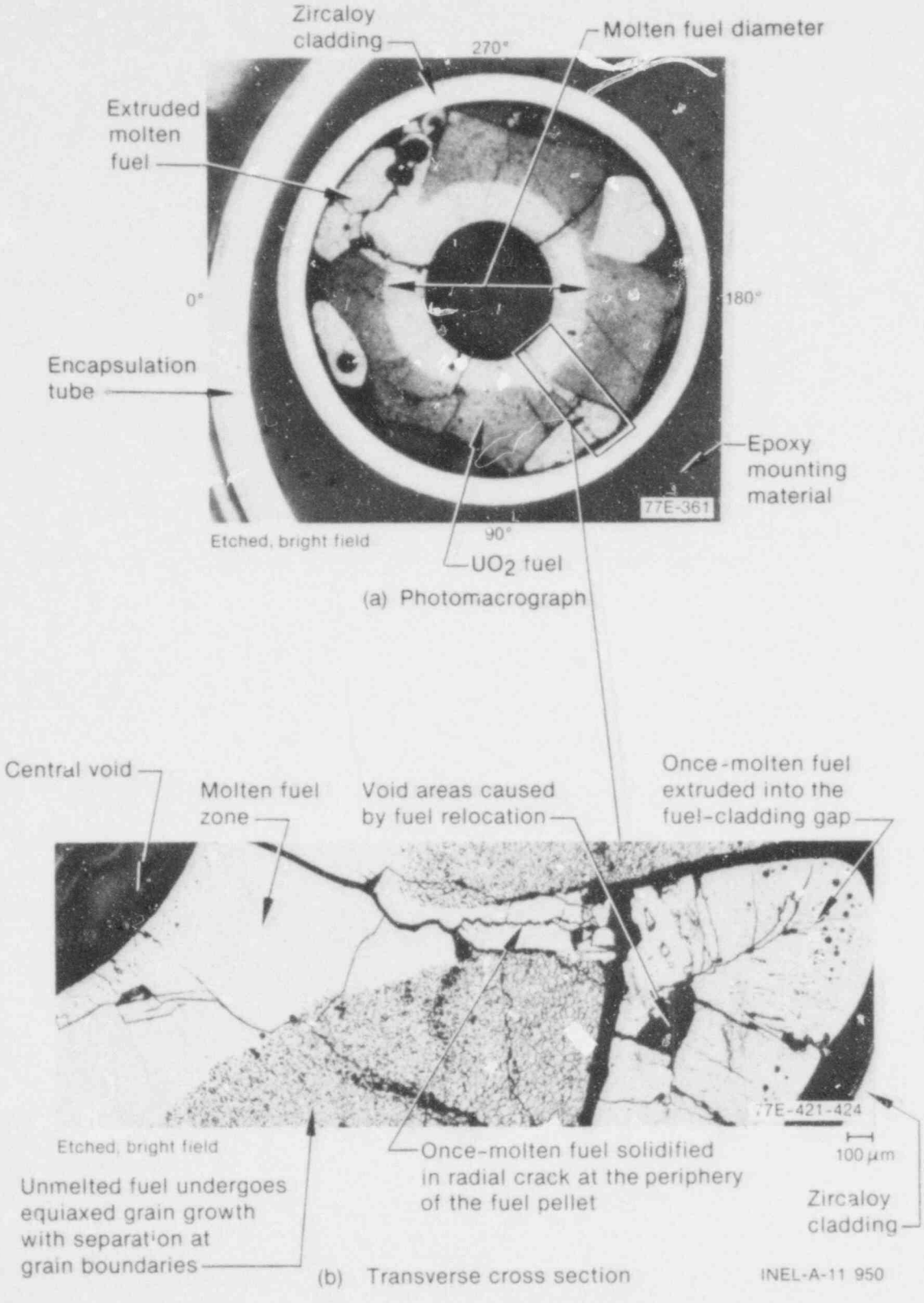

Fig. 11 Molten fuel radial extrusion into fuel-cladding gap observed during PCM in-pile test[6].

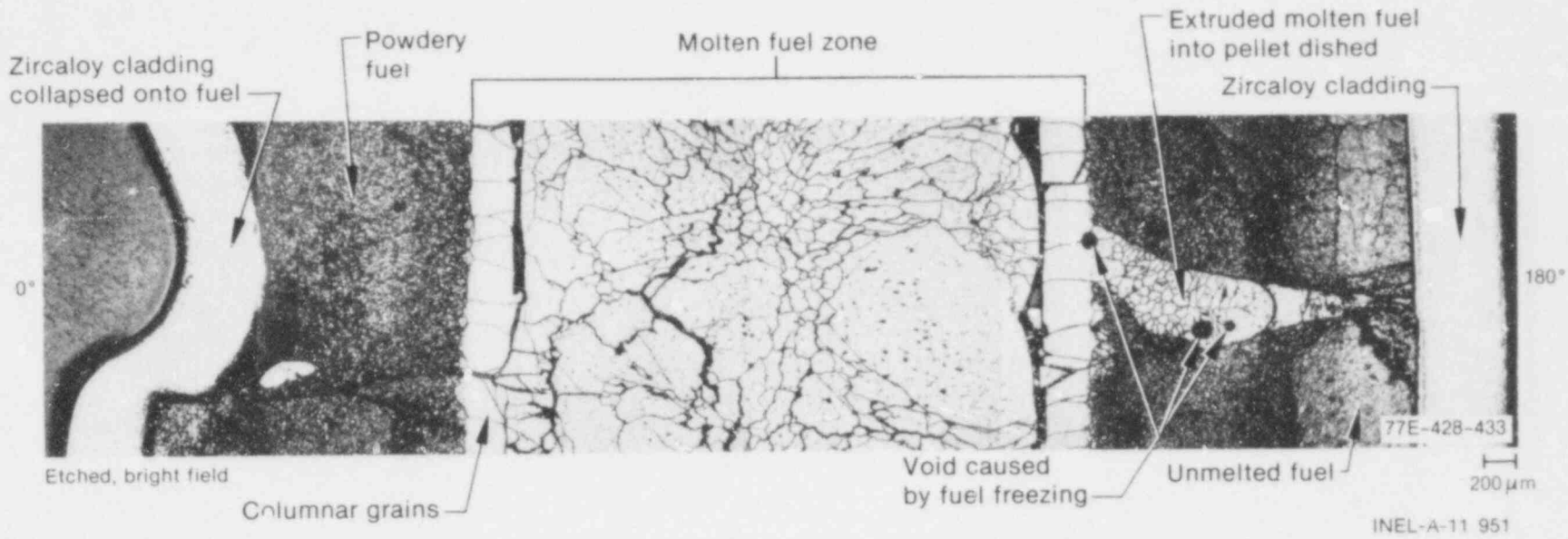

Fig. 12 Fuel microstructure and molten fuel extrusion into pellet dishes observed during PCM in-pile test[6].

4. DRIVING FORCES FOR RADIAL EXTRUSION OF MOLTEN FUEL

If fuel melting occurs at the center of the pellet during a PCM event, molten fuel may extrude through radially open cracks in the outer, unmelted portion of the fuel pellet (characterized earlier) and relocate in the fuel-cladding gap. A differential pressure between the central melting zone and the fuel-cladding gap is required to cause this extrusion. The pressure in the fuel-cladding gap and gas plenum increases with increasing operating power as shown in Figure 13 for a typical pressurized water reactor fuel rod during a PCM in-pile test[21]. The pressure at the center of the rods, however, is caused by the several factors discussed subsequently.

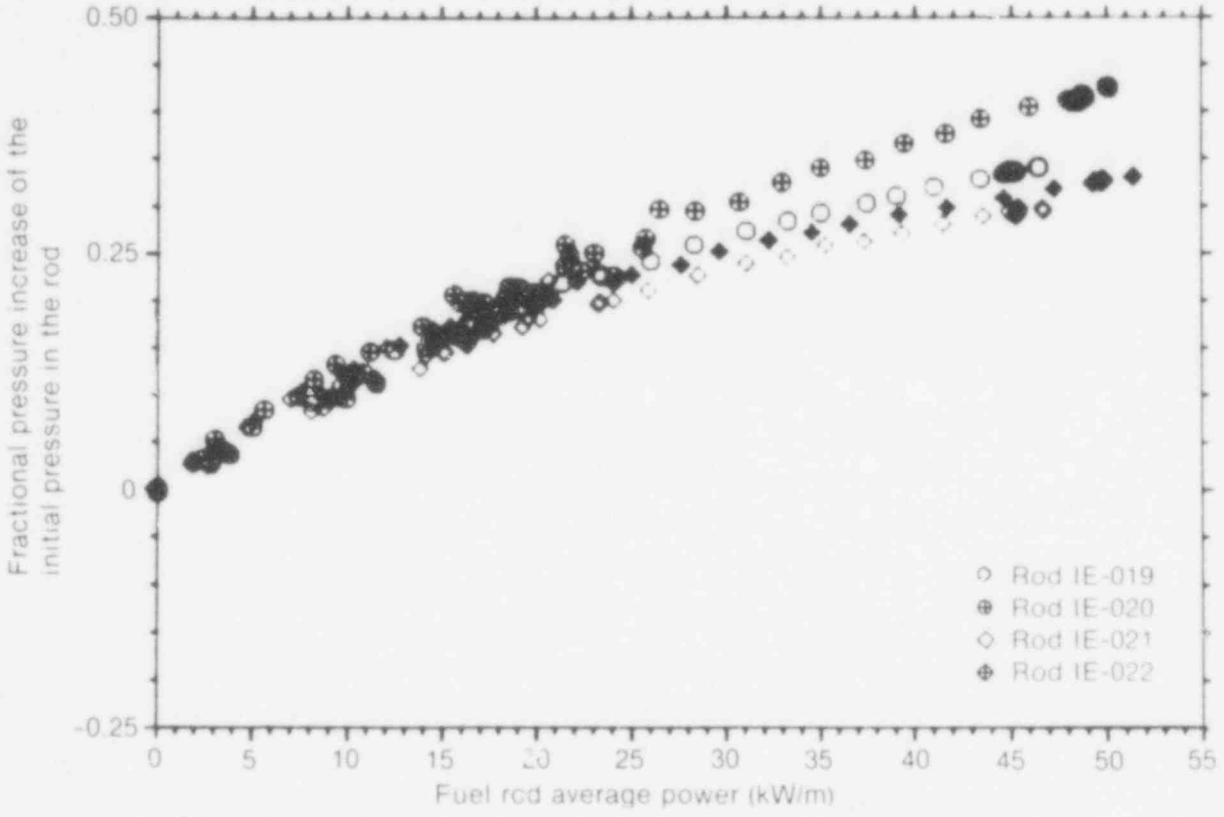

Fig. 13 Internal pressure increase for unirradiated fuel rod as a function of the average operating power.

First, if good wetting characteristics are assumed between molten and solid UO_2 [a], a capillary pressure[24] would be present due to the small width of the radial cracks. Second, a pressure would be induced by the volumetric expansion of UO_2 fuel due to both melting[b], which is about 3.6% for fuel of 94% theoretical density, and due to the thermal expansion of the molten fuel as the temperature increases above the melting point (~0.0105% volume increase per degree of superheat[18]). Third, fission gases present in irradiated fuel will migrate toward the fuel centerline during operation. In conjunction with sintering, a void will form at the centerline of the pellet. If a PCM event occurs in which fuel melting at the

a. Livey and Murray[22] have indicated that solid oxides are readily wetted by molten oxides, with the angle of contact invariably less than 90 degrees. Increasing the system temperature would, however, decrease the angle of contact[23]; that is, complete wetting would take place.

b. The decrease in density of a UO_2 single crystal upon melting has been found to be approximately 9.6%[17]. The density of the solid UO_2 at 3073°C was 9.67 ± 0.13 g/cm^3; that of the molten UO_2 at 3073°C was 8.74 ± 0.16 g/cm^3.

center of the pellet is initiated, fission gases will be released from the fuel matrix as it melts, forming a void at the center of the pellet. The central void may be pressurized by hot fission gases if the molten fuel seals cracks in the pellet due to fuel solidification on the crack walls. A fourth driving force for the fuel extrusion is the fuel vapor pressure. The UO_2 vapor pressure as a function of the inverse of the fuel temperature is shown in Figure 14. As indicated in the figure, the vapor pressure of the molten UO_2 fuel, superheated 500 K, is ~0.1 MPa. In a PCM event, since the maximum superheating of molten fuel at the center of the pellet is not expected to exceed 500 K, the contribution from the vapor pressure should be less than 0.1 MPa. This situation would tend to create a force on the molten fuel to extrude through the radially open cracks and relocate in the fuel-cladding gap.

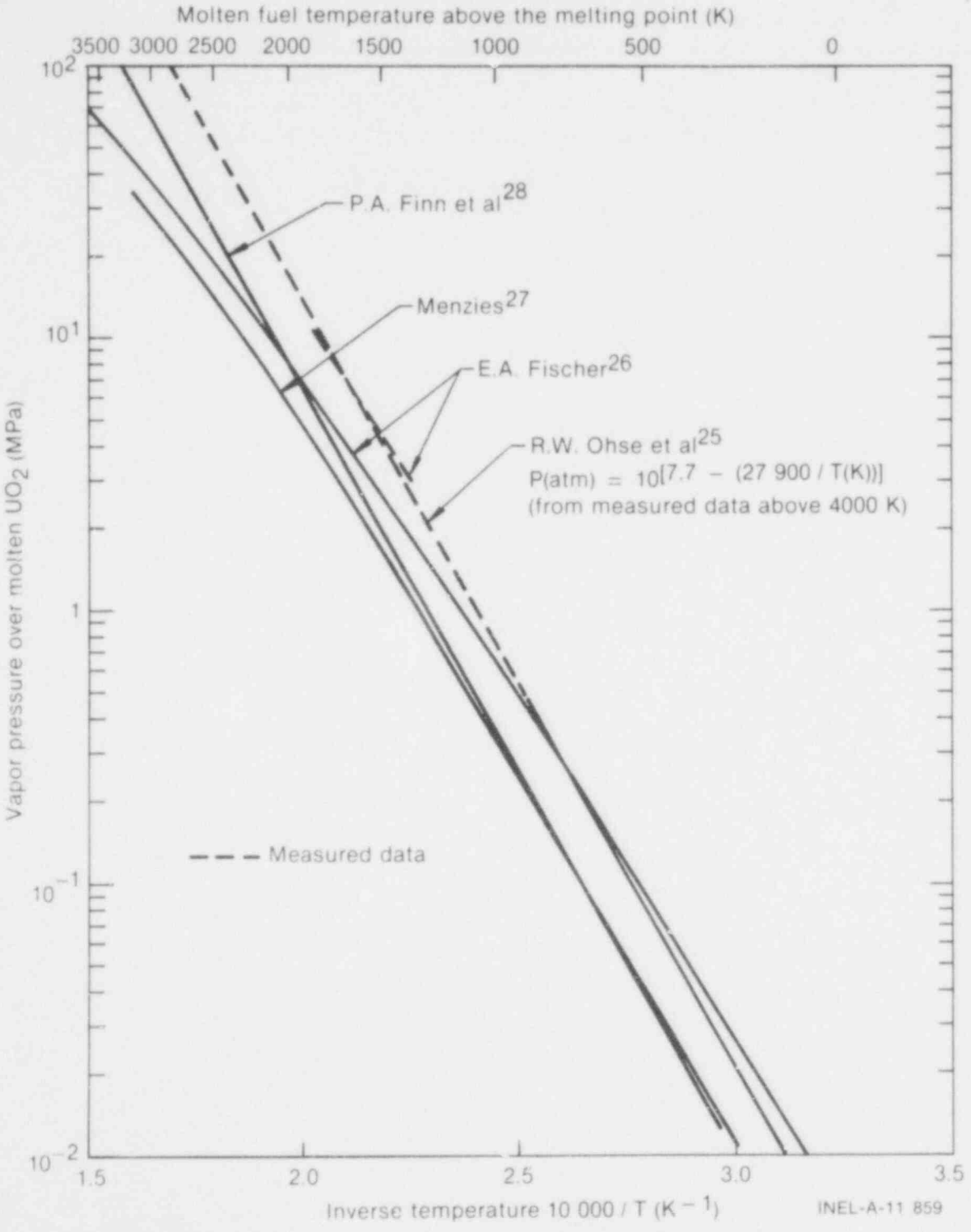

Fig. 14. UO_2 vapor pressure as a function of the inverse of the fuel temperature.

III. SOLIDIFICATION OF A SUPERHEATED LIQUID PENETRATING AN INITIALLY EMPTY CRACK WITH APPLICATION TO IN-PILE EXPERIMENTS

In this section, the transient solidification of a superheated liquid penetrating a short, initially empty crack is studied analytically and applied to fuel performance in LWRs during a PCM event. A closely related study is introduced in Reference 29 for the transient freezing of a liquid as it penetrates a long, initially empty, cold channel or tube. Cheung and Baker[30] conducted a series of experiments in which various liquids were allowed to flow under gravity into long copper tubes cooled by liquid nitrogen or by a dry ice-acetone bath. The penetration distances were measured as functions of constant driving heads in the liquid reservior. The solidification of a saturated liquid as it penetrates an initially empty tube, maintained at a constant subfreezing temperature, is treated theoretically and experimentally in Reference 31. Epstein and Hauser[32] extended this work for a convectively cooled tube, in which the theory was compared with experiment. They concluded that better agreement between the theory and experiment could be obtained by using a more accurate solidification model than the one they used in analysis[33]. A simple solution was introduced by Madejski[34] for the penetration and freezing of a saturated liquid through channels and into cavities. His analysis is based on the assumption that the pressure drop over the liquid penetration length is the same as for a fully developed flow.

These analyses[31,32,34] are generally limited to those cases in which the liquid is saturated and the change in liquid density upon freezing is negligible. This restricts the validity of such work, since the extruded molten fuel during a PCM event might be superheated, and the change of molten UO_2 density upon freezing is about 11 to 15%, depending on the temperature of the molten fuel, which might affect the accuracy of the predictions. The purpose of the current analysis is to provide a physical model for the transient freezing of a superheated liquid as it penetrates a short, initially empty crack maintained at a constant subfreezing temperature. In this analysis the thermophysical properties in the solidified crust and in the liquid are considered constant but different, thereby accounting for any difference in density upon freezing. The transient behavior of the deposited crust on the crack walls and of the liquid penetration is presented graphically in a dimensionless form, varying the governing parameters; namely, driving pressure, crack shape, density factor, Stefan number for freezing, and steady state crust thickness. The calculational results are applied to PCM in-pile experiments in which radial extrusion of molten UO_2 has been observed.

1. PHYSICAL MODEL

A schematic representation of the physical model and coordinate system for the transient freezing of a superheated liquid as it penetrates an initially empty crack is shown in Figure 15. At time zero the liquid is allowed to flow and enter an empty crack maintained at a constant subfreezing temperature, T_w. The following assumptions are imposed for simplification of the analysis.

(1) The temperature at the liquid-solid interface is constant and equal to the freezing temperature of the liquid.

(2) The liquid and the solidified crust have constant but different thermophysical properties.

(3) The inertia of the liquid is neglected.

(4) The liquid outside the crack entrance has a zero approach velocity.

(5) Axial heat conduction within the frozen crust is negligible and the crack walls are maintained at a constant subfreezing temperature (that is, isothermal wall). These assumptions imply that the crust is thin compared with its extension in the direction of the flow, and that the crust thickness is maximum at the crack entrance (that is, at $z = 0$).

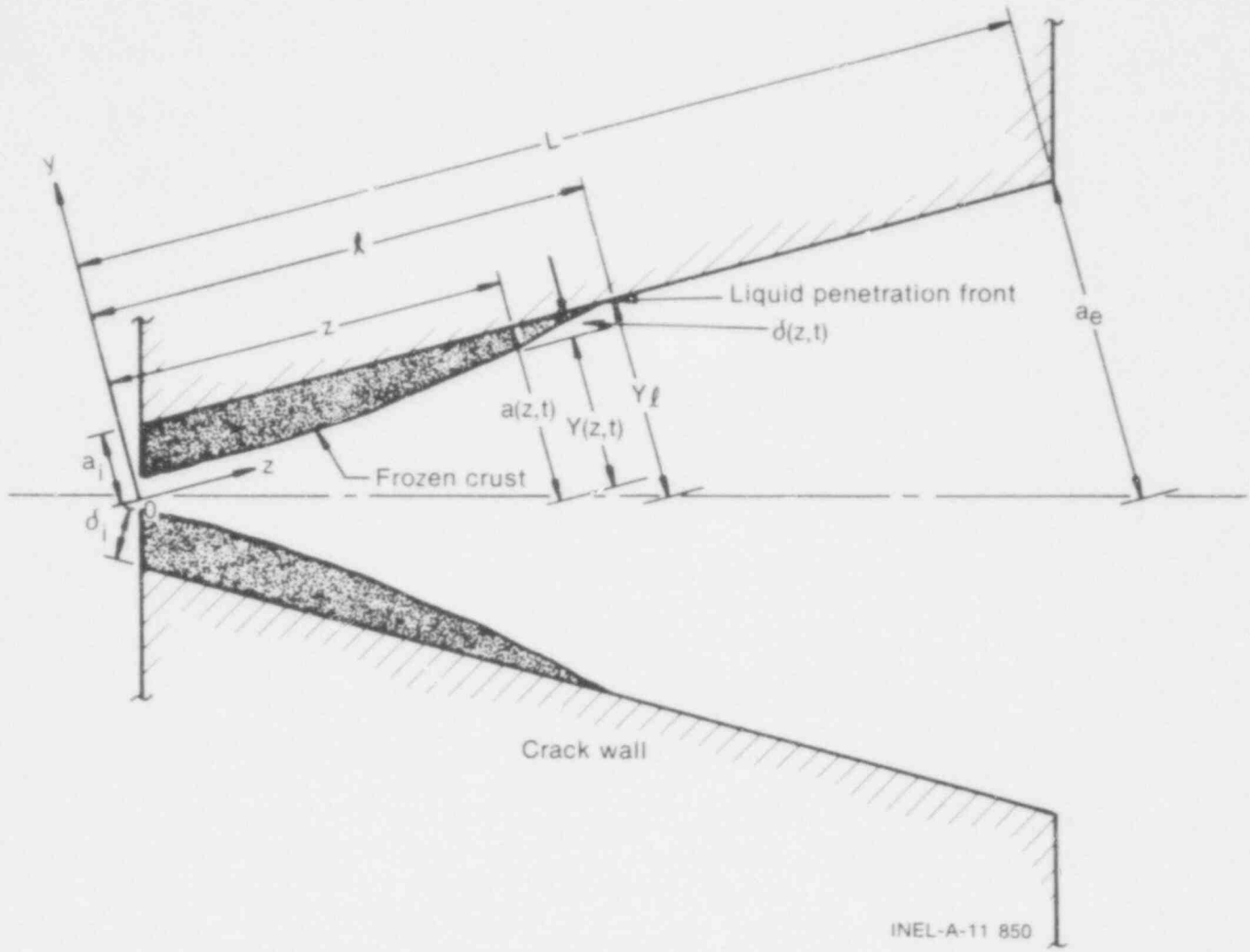

Fig 15 Schematic representation of physical model and coordinates system for freezing of a superheated liquid penetrating a divergent, initially empty crack maintained at a constant, subfreezing temperature.

(6) The axial variation of the flow area, as a function of time Y(z,t), is described by a function of the form[35]

$$\frac{Y(z,t)}{Y_\ell} = \left\{1 - \left[1 - \left(\frac{a_i - \delta_i}{Y_\ell}\right)\right]\left(1 - \frac{z}{\ell}\right)^n\right\}. \tag{4}$$

The exponent, n, appearing in Equation (4) takes on values in the range $0 \le n \le 1$. When $n = 0$, the solidified crust would deposit uniformly on the crack walls. A square root solidification profile and a linear profile would be obtained for $n = 1/2$ and 1, respectively. The crust profile for $n = 1/2$ is considered in the present work, since it has been verified theoretically using a numerical approach[35], which showed good agreement in the special case of an isothermal wall, which is the assumption in the present analysis [Assumption(5)].

(7) For turbulent flow conditions (Reynolds number, Re, $> 5 \times 10^2$), circular tube correlations are used to represent the friction coefficient and the convective coefficient of heat transfer between the liquid and the frozen crust by employing the hydraulic diameter in Reynolds and Nusselt numbers[36].

(8) The bulk temperature of the liquid, T_b, is assumed constant along the entire penetration length through the crack.

2. ANALYSIS

In this section the equations governing the transient freezing and penetration of the liquid into a short, initially empty crack are derived, taking into account the assumptions in the previous section. Through the use of Equation (4), the following time-dependent profile for the solidified crust deposited on the crack walls is obtained:

$$\delta(z,t) = \left[a_i\, \gamma\, \left(\frac{\ell}{L}\right) + \delta_i\right]\left(1 - \frac{z}{\ell}\right)^n - a_i\, \gamma\, \left(\frac{\ell}{L}\right)\left(1 - \frac{z}{\ell}\right). \tag{5}$$

The case for $\gamma = 0$ represents a flat slit ($a_i = a_e$), whereas $-1 \le \gamma < 0$ represents a convergent crack ($0 < a_e < a_i$) and $\gamma > 0$ represents a divergent crack ($a_i < a_e$).

The present analysis is furnished in a dimensionless form, using the dimensionless parameters listed in Table II, as to be applicable to a general class of problems of engineering utility rather than for a specific example. Through use of these dimensionless parameters, Equation (5) is written in a dimensionless form as

$$\Delta(z,t) = (\gamma\Phi + \Delta_i)\left(1 - \frac{\ell}{L}\right)^n - \gamma\Phi\left(1 - \frac{\ell}{L}\right). \tag{6}$$

The volume of the solidified layer, W_s, considering one half of the crack and a unit depth, is given by

$$W_s(\tau) = \int_0^\ell \delta(z,\tau)\,dz = \Phi(a_i L)\left[\left(\frac{\gamma\Phi - \Delta_i}{1+n}\right) - \frac{1}{2}\gamma\Phi\right]. \tag{7}$$

For the geometry considered, the filled volume is equal to

$$W_T(\tau) = \int_0^\ell a(z,t)\,dz = (a_i L)\left(1 + \frac{\gamma}{2}\Phi\right). \tag{8}$$

TABLE II

DIMENSIONLESS PARAMETERS

$A \equiv \left(\frac{\Delta P}{\rho_m}\right)\left(\frac{a_i^2}{L}\right)^2$	(dimensionless pressure),	$\Phi \equiv \frac{\ell(t)}{L}$	(dimensionless penetration length),
$\alpha = (\nu/\alpha_{sf})$	(kinematic viscosity - thermal diffusivity ratio),	$\psi_i \equiv (v_i a_i^2/\nu L)$	(dimensionless velocity at the crack entrance),
$\beta \equiv \frac{(1-\Delta_i)}{(1+\gamma\Phi)}$	(flow ratio at the crack entrance),	$\tau \equiv \left(\frac{\nu t}{a_i^2}\right)$	(dimensionless time),
$\Delta_i \equiv \frac{\delta_i(t)}{a_i}$	(dimensionless thickness of the crust at the crack entrance),	$\varepsilon \equiv \frac{\rho_s - \rho_m}{\rho_m}$	(density ratio),
$\Delta \equiv \frac{\delta(z,t)}{a_i}$	(dimensionless thickness of the crust),	$SN \equiv \frac{c\rho_s(T_f-T_w)}{h_f}$	(Stefan number),
$\Delta_{ss} \equiv \frac{k_s(T_f-T_w)}{h(T_b-T_f)a_i}$	(dimensionless steady state thickness of the crust),	$\gamma \equiv \frac{(a_e - a_i)}{a_i}$	(crack shape factor).

The total mass, m, of the liquid allowed to flow into the crack from time $\tau = 0$ to τ is then

$$m = \rho_s W_s + \rho_m (W_T - W_S) = \rho_m a_i L \int_0^{\tau} \psi_i \quad (1 - \Delta_i) \quad d\tau . \tag{9}$$

Rearrangement and differentiation of Equation (9) once with respect to τ results in

$$B_i(\tau) \quad \frac{d\Phi}{d\tau} = \psi_i \left(1 - \Delta_i\right) - \left(\frac{\varepsilon \Phi}{1+n}\right) \quad \frac{d\Delta_i}{d\tau} \tag{10}$$

where

$$B_i(\tau) = \left\{1 + \gamma\Phi \left[1 - \varepsilon + \left(\frac{2\varepsilon}{1+n}\right)\right] + \left(\frac{\Delta_i \varepsilon}{1+n}\right)\right\} . \tag{11}$$

Equation (10) gives the dimensionless velocity of the liquid at the penetration front in terms of the transient parameters at the crack entrance; namely, the solidified crust thickness, Δ_i; the freezing velocity of the crust, $d\Delta_i/d\tau$; and the liquid flow velocity, ψ_i.

For the freezing of a superheated liquid flowing over an isothermal wall [Assumption (5) from the previous subsection], the exact analytical expression for the freezing velocity in a dimensionless form is as follows[37]:

$$\frac{d\Delta}{d\tau} = SN \left[\sqrt{\frac{\alpha}{\pi\tau}} \quad \frac{e^{-(\Delta^2 \alpha/4\tau)}}{\operatorname{erf}\left(\frac{\Delta}{2}\sqrt{\frac{\alpha}{\tau}}\right)} - \frac{1}{\Delta_{ss}} \right] . \tag{12}$$

It is noted that for the freezing of a saturated liquid (that is, $\Delta_{ss} = \infty$), the second term in Equation (12) becomes zero and $\Delta(\tau)$ is given by the relation

$$\Delta(\tau) = 2\lambda\sqrt{(\tau/\alpha)} \tag{13}$$

where λ is the freezing constant evaluated from the transcendental equation[38]

$$SN = \lambda\sqrt{\pi} \cdot \operatorname{erf}(\lambda) \cdot e^{\lambda^2} . \tag{14}$$

To determine the liquid flow velocity at the crack entrance, a generalized mechanical energy balance, in which the liquid inertia is neglected [Assumption (3) from the previous subsection], is written as

$$0 = \begin{bmatrix}\text{net rate of}\\ \text{change in}\\ \text{kinetic}\\ \text{energy}\end{bmatrix} + \begin{bmatrix}\text{net rate of}\\ \text{work accom-}\\ \text{plished due}\\ \text{to pressure}\\ \text{forces}\end{bmatrix} + \begin{bmatrix}\text{net rate of}\\ \text{work accom-}\\ \text{lished due}\\ \text{to friction}\\ \text{forces}\end{bmatrix} + \begin{bmatrix}\text{net rate of}\\ \text{energy loss}\\ \text{due to flow}\\ \text{momentum}\\ \text{change}\end{bmatrix}$$

$$0 = \nabla \left(\frac{\rho_m v^2}{2}\right) + \nabla P + K \left(\frac{\rho_m v^2}{2}\right) + (\rho_m v^2) . \tag{15}$$

The last term in the preceding equation represents the liquid momentum loss because of the nonuniformity of the flow area along the penetration length of the liquid caused by the crack shape and the deposition of the frozen crust on the crack walls.

By application of Equation (15) between the surface of the accumulated liquid outside the crack and the entrance of the crack, the liquid inlet velocity, v_i, is determined as

$$v_i^2 \quad (3 + K_c) = \frac{2}{\rho_m} (P_o - P_i) \quad . \tag{16}$$

Again, the energy balance between the crack entrance and the liquid penetration front within the crack (that is, at $z = l$), making use of Equation (16), can be expressed as

$$v_i^2 \left[3\beta^2 \quad + K_c + K_f \right]_i = 2 \frac{(P_o - P_g)}{\rho_m} \quad . \tag{17}$$

The friction loss coefficient, K_f, in Equation (17) can be generally expressed as

$$K_f = \frac{\ell \cdot f}{a_i (1 - \Delta_i)} \quad . \tag{18}$$

For a turbulent flow[36], the friction factor, f, takes the form

$$f = C_1 (Re)^{C_2} \tag{19}$$

where

$$\left.\begin{array}{lcl} C_1 & = & 0.079 \\ C_2 & = & -0.025 \end{array}\right\} \text{ for } 5 \times 10^3 \leq Re \leq 3 \times 10^4$$

and (20)

$$\left.\begin{array}{lcl} C_1 & = & 0.046 \\ C_2 & = & 0.2 \end{array}\right\} \text{ for } 3 \times 10^4 \leq Re \leq 10^6 .$$

For a laminar flow, however, f is taken to be[36]

$$f = \left(\frac{24}{Re}\right) . \tag{21}$$

The substitution of Equation (18) into Equation (17) results in an implict expression for v_i, which can be evaluated numerically.

For turbulent flow, such an expression written in a dimensionless form is

$$\psi_i^2 \left[3\left(\frac{1-\Delta_i}{1+\gamma\Phi}\right)^2 + K_c \right] + \left[\frac{(4)^{C_2} C_1 \cdot \Phi}{(1-\Delta_i)^{1-C_2}} \right] \left(\frac{L}{a_i}\right)^{1+C_2} \left(\psi_i\right)^{2+C_2} - 2A = 0. \quad (22)$$

For laminar flow, Equation (17) becomes

$$\psi_i^2 \left[3\left(\frac{1-\Delta_i}{1+\gamma\Phi}\right)^2 + K_c \right] + \frac{6\Phi}{(1-\Delta_i)^2} \psi_i - 2A = 0. \quad (23)$$

For a short penetration length into the crack (that is, for $\Phi << 1$), the dimensionless flow velocity at the crack entrance takes an identical simplified form for both turbulent and laminar flow, as

$$\psi_i(\tau) \simeq \sqrt{\frac{2A}{3(1-\Delta_i)^2 + K_c}} \quad (24)$$

which reduces to a constant velocity for $\Delta_i \simeq 0$ (that is, without significant liquid freezing), as

$$\psi_c = \left[\frac{2A}{(3 + K_c)} \right]^{1/2} . \quad (25)$$

For a longer penetration length in the crack (that is, for $\Phi \simeq 1$), however, the first terms in Equations (22) and (23) could be neglected in favor of the second term, which results in the following simplified expressions for the dimensionless flow velocities at the crack entrance:

(a) For turbulent flow:

$$\psi_i(\tau) = \left[\frac{2A(1-\Delta_i)^{1-C_2}}{(4)^{C_2} C_1 \cdot \left(\frac{L}{a_i}\right)^{1+C_2}} \right]^{\frac{1}{2+C_2}} \quad 26)$$

(b) For laminar flow:

$$\psi_i(\tau) = \left(\frac{A(1-\Delta_i)^2}{3\Phi} \right) . \quad (27)$$

A general expression for the dimensionless flow velocity at the crack entrance, considering a laminar flow, is obtained through the rearrangement of Equation (23), which gives the following simplified expression for ψ_i, as:

491 039

$$\psi_i(\tau) = 3E\left[-1 + (1 + \frac{2}{9}\ A\ F)^{1/2}\right] \tag{28}$$

where

$$E = \Phi\left[3\ \frac{(1-\Delta_i)^4}{(1+\gamma\Phi)^2} + K_c(1-\Delta_i)^2\right]^{-1}$$

and

$$F = (1-\Delta_i)^2 / E\Phi. \tag{29}$$

The convective coefficient of heat transfer, h, for a turbulent flow can be obtained through the use of the Seban and Shimazak formula[36] for molten-like fluids flowing in a circular channel with constant temperature in the channel wall

$$h = 4.8 + 0.025\ Pe^{0.8}\ . \tag{30}$$

For laminar flow in a rectangular duct, in which the depth of the duct is much larger than the width[36],

$$h = \left(\frac{k_m}{a_i}\right)\ \frac{1.885}{(1-\Delta_i)}\ . \tag{31}$$

The coupling of Equations (10), (12), (22), and (30) represents a complete mathematical model of the transient freezing of a superheated liquid as it penetrates an initially cold, empty crack where the flow is turblent. Such coupling is adequate to determine the three unknown functions, $\Delta_i(\tau,A,\varepsilon,SN,\gamma,\Delta_{ss})$, $\Phi(\tau,A,\varepsilon,SN,\gamma,\Delta_{ss})$, and $\psi_i(\tau,A,\varepsilon,SN,\gamma,\Delta_{ss})$ subject to the initial conditions $\Delta_i(\tau=0) = 0$, $\Phi(\tau=0) = 0$, and $\psi_i(\tau=0) = \psi_c$; ψ_c is given from Equation (25) . For a laminar flow, however, Equations (22) and (30) are replaced by Equations (28) and (31), respectively.

3. RESULTS AND DISCUSSION

The approximate analytical model developed in the previous subsection for the transient freezing of a superheated liquid penetrating an initially empty crack maintained at constant subfreezing temperature is applied herein, considering laminar flow conditions. A parametric study of the effect of various dimensionless groups on the multiple freezing-penetration processes of the liquid is evaluated and demonstrated graphically. The dimensionless groups of interest are: the driving pressure, A; crack shape factor, γ; density ratio, ε; and the steady state frozen crust thickness, Δ_{ss}. The conditions considered for the reference case are as follows:

$A = 100$	$SN = 2$
$\gamma = 0$	$\Delta_{ss} = 10$
$\varepsilon = 0$	$\alpha = 1$

As shown in Figure 16, the initial velocity of the liquid at the crack entrance, ψ_i, is essentially constant, since it is primarily ruled at such early time solely by the dimensionless driving pressure, A, [Equation (25)]. Then, the acceleration force induced at the crack entrance because of the change of liquid kinetic and momentum energies causes ψ_i to increase with time until it reaches a maximum value, when the

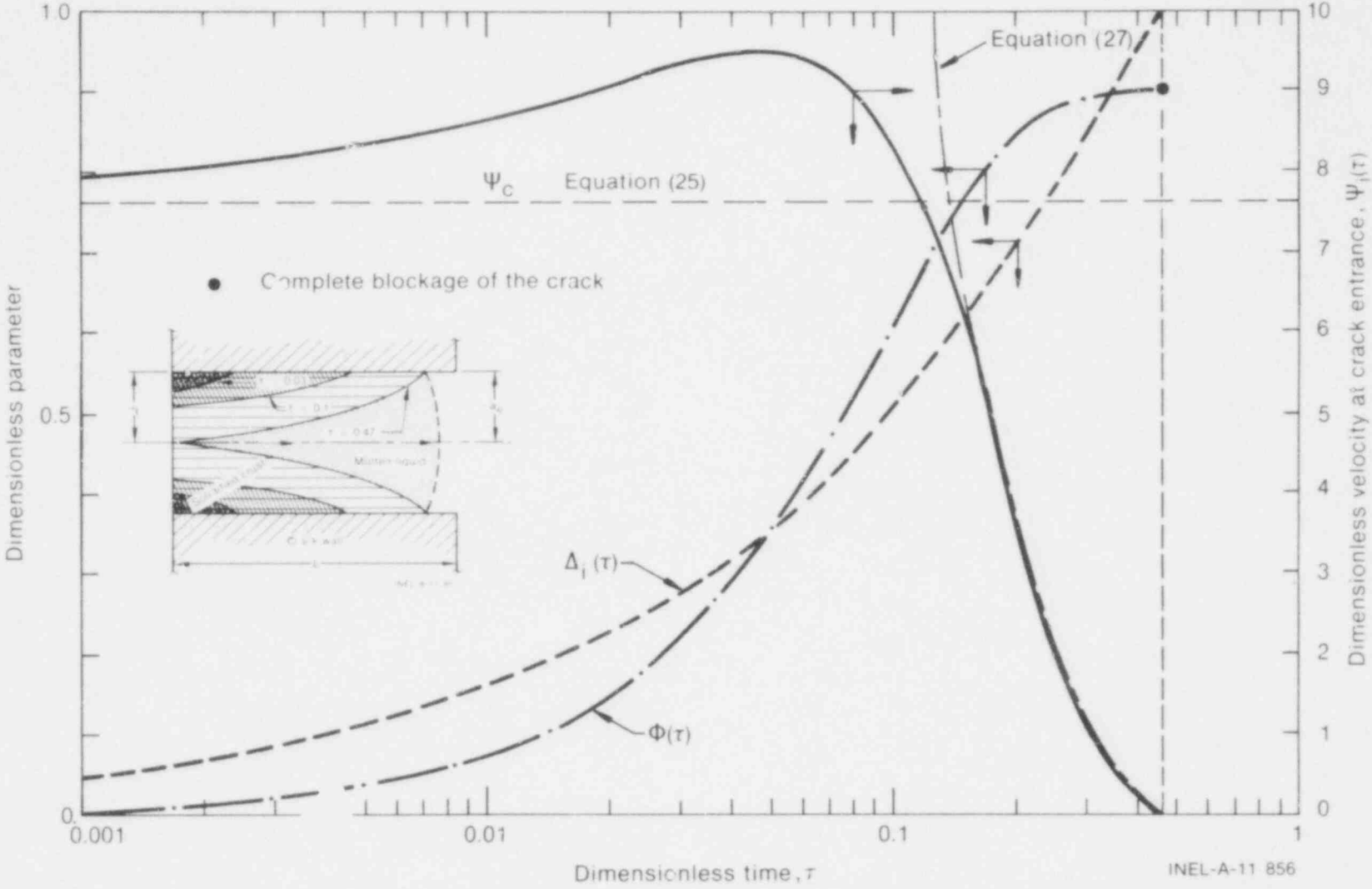

Fig. 16 Transient behavior of the dimensionless parameters for the reference case problems.

loss of pressure due to friction balances that due to the liquid acceleration. After that time however, the pressure loss due to friction becomes greater and forces the velocity of the liquid at the crack entrance to decline with time. The velocity ultimately approaches zero when the crack entrance is completely blocked by the freezing of the liquid on the crack walls. The liquid penetration into the crack thereby comes to a complete stop.

The effect of both the dimensionless pressure, A, and the crack shape factor, Y, on the maximum penetration length of the liquid before complete blockage of the crack occurs, $\Phi_{blockage}$, is demonstrated in Figure 17. As indicated, for a negative shape factor of the crack (that is, a convergent crack) $\Phi_{blockage}$ is greater than that for the cases where Y is either zero (that is, a parallel wall crack) or positive (that is, a divergent crack). The former case represents a crack shape typical of that at the pellet dishes. The latter case, however, represents a crack shape typical of that which usually forms at the periphery of the pellet during reactor operation.

The effect of the liquid density change upon freezing on $\Phi_{blockage}$ is demonstrated in Figure 18. As indicated, a change of $\pm 20\%$ in liquid density results in a respective error of -8% to +10% in predicting the penetration length of the liquid, $\Phi_{blockage}$. This reflects the importance of considering such a change of liquid density upon freezing in the application to molten UO_2 fuel (discussed in the next section), for which $\varepsilon \approx 11$ to 15%.

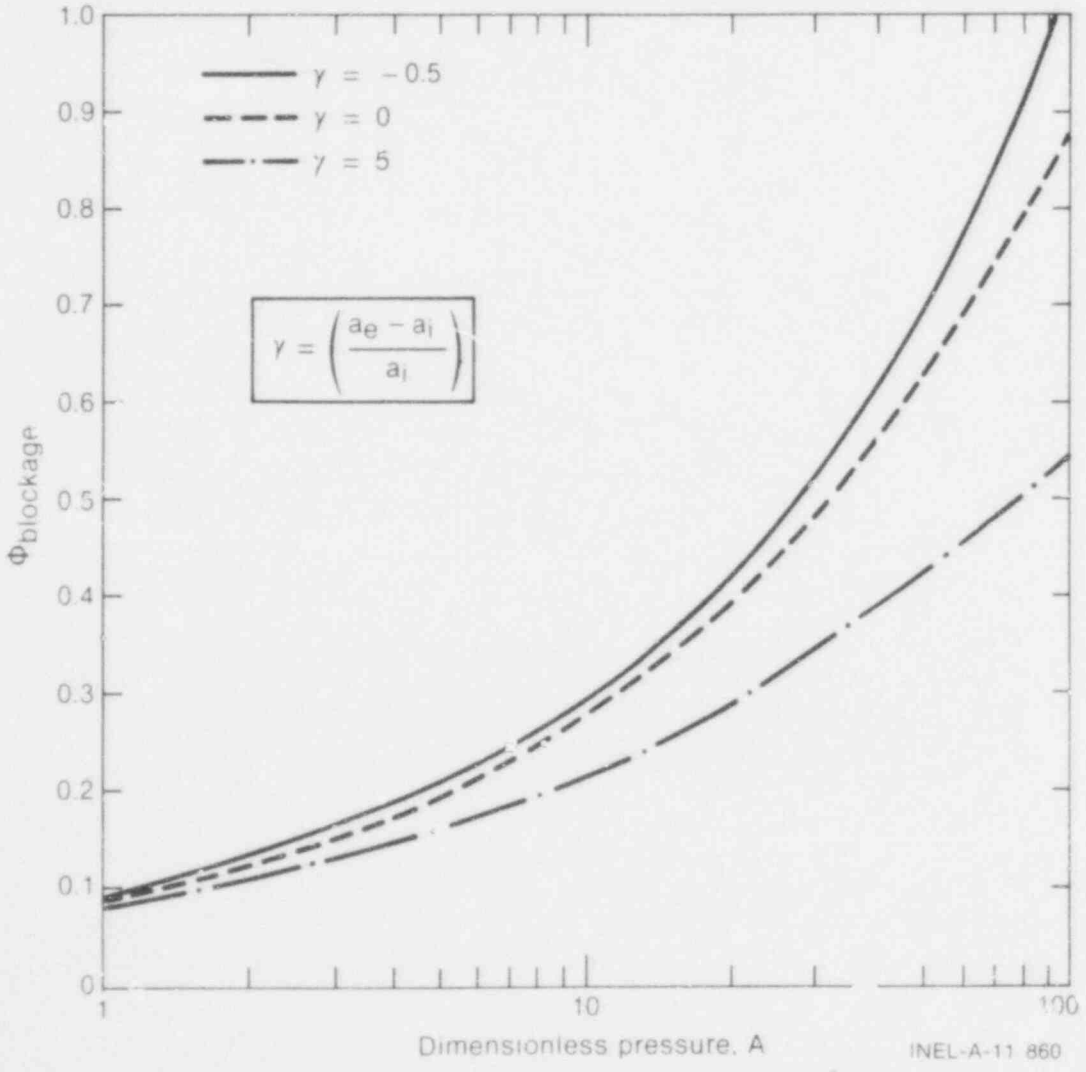

Fig. 17. Effect of crack shape and driving pressure on the liquid maximum penetration length.

491 042

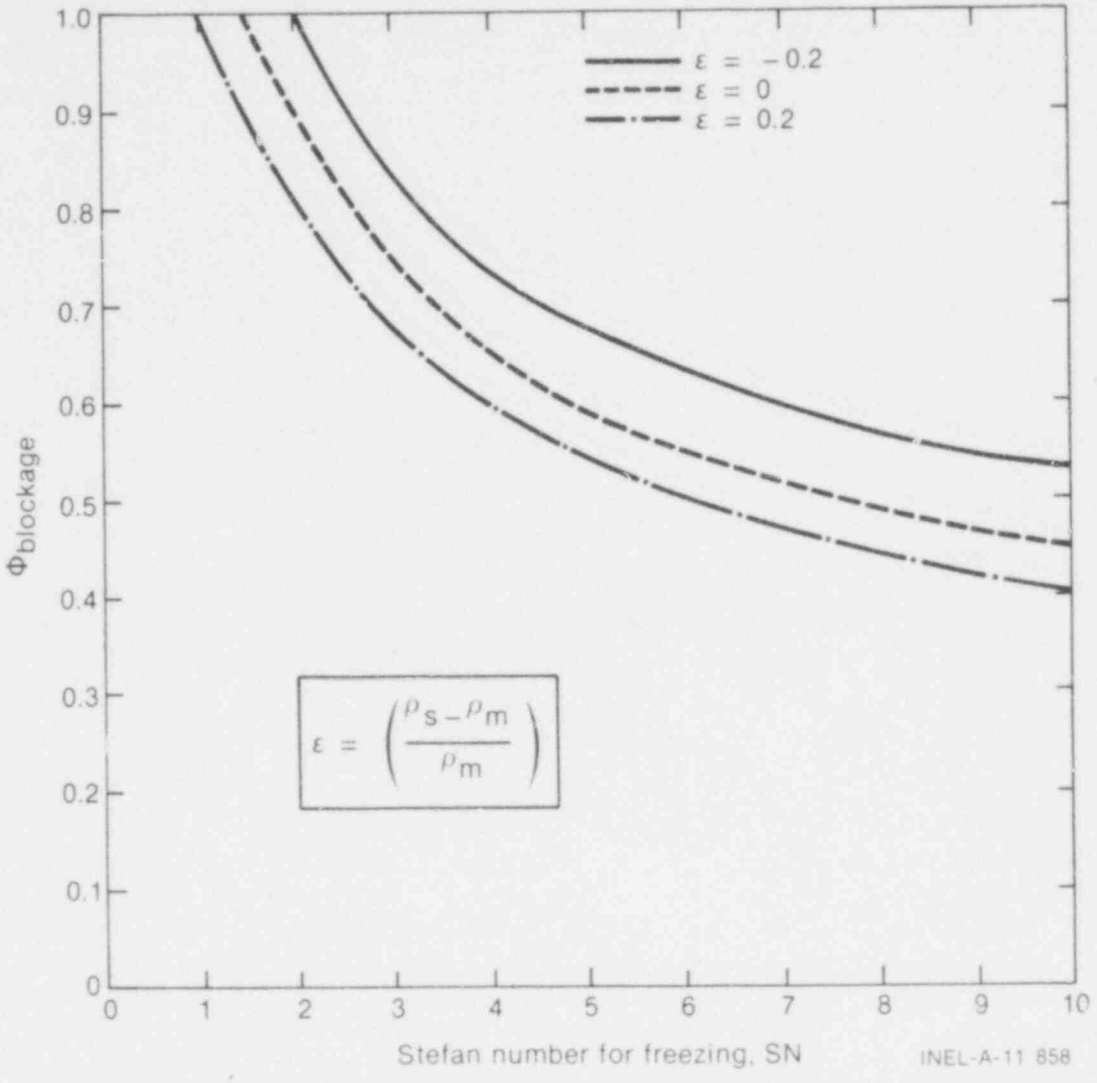

Fig. 18 Effect of liquid density change upon freezing on the maximum penetration of the liquid through the crack.

The liquid temperature, the subfreezing in crack walls, and the liquid flow conditions are all important in determining whether or not crack blockage might occur before the liquid can penetrate through the entire length of the crack. An answer is demonstrated in Figure 19, in which increasing the wall subfreezing temperature (that is, increasing SN) or decreasing the liquid superheating or flow conditions (that is, increasing Δ_{SS}) would result in a faster growth rate of the frozen crust, and ultimately an earlier blockage of the crack before the liquid can penetrate the entire length of the crack. Decreasing Δ_{SS}, however, produces an asymptotic frozen crust on the crack wall which grows with time until it reaches a steady state thickness of less than half of the crack opening. In this case, the liquid would continue to flow through the crack since complete crack blockage is not obtainable. Therefore, neglecting liquid flow or superheating, as has been the case in previous analyses[31,32,34], will underpredict the liquid penetration length and the blockage time of the crack.

The results of this parametric study demonstrate that the liquid penetration process into an initially empty crack depends mainly on the driving pressure across the crack, the crack length, and the crack shape (that is, a divergent, a parallel wall, or a convergent crack). However, the transient growth of the deposited crust on the crack walls is mainly governed by the subfreezing in the wall and the superheating in the penetrating liquid. For a liquid at its fusion temperature, the frozen crust continues to grow with time until it eventually induces complete blockage of the crack. When the liquid is superheated, however, the growing crust approaches a steady state thickness which might be less than the half width of the crack opening. In

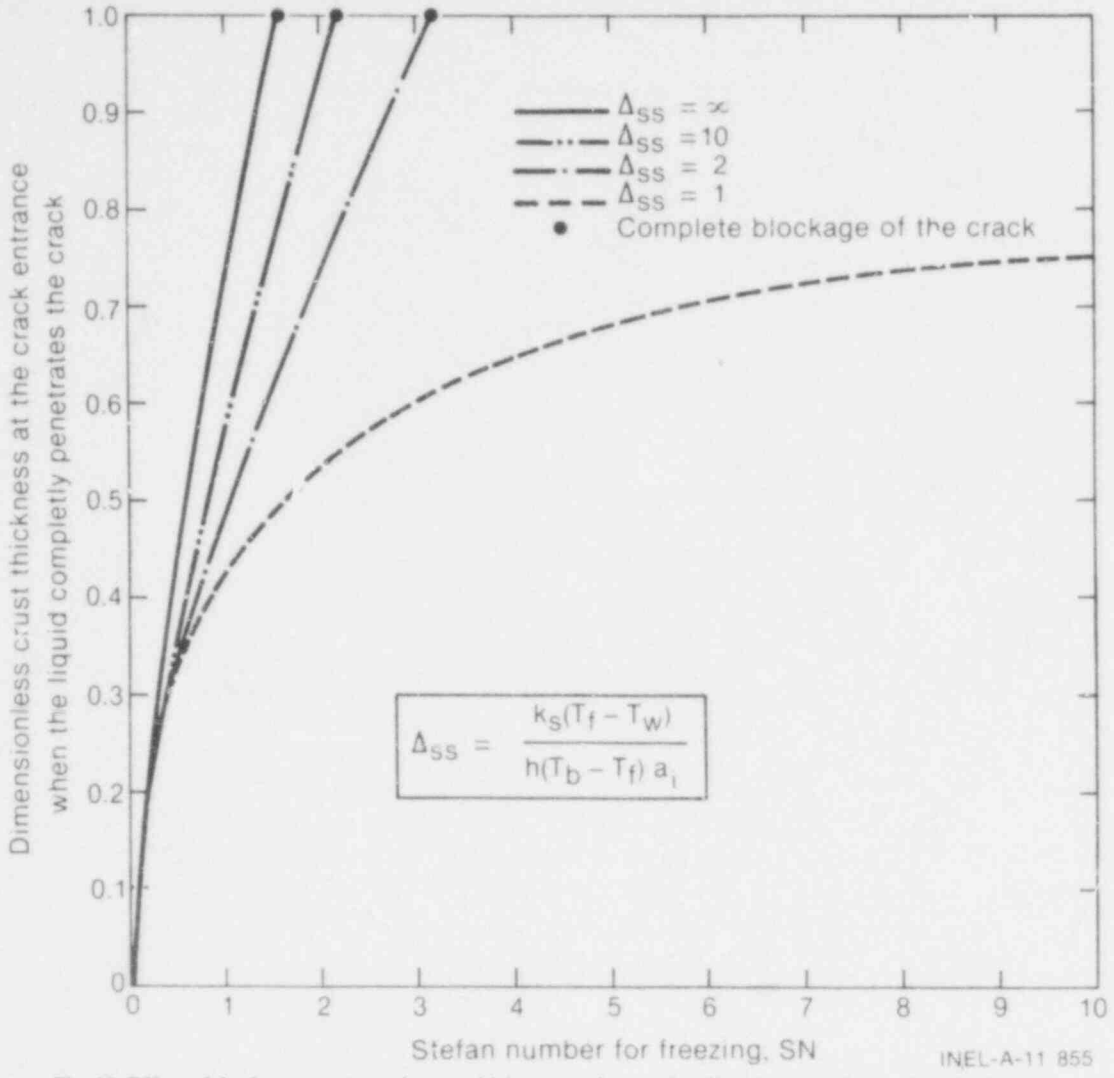

Fig. 19 Effect of the frozen crust steady state thickness on the transient liquid penetration and crack blockage.

this case, complete blockage of the crack is impossible; only partial blockage would occur. In the next subsection the calculational results are applied to molten UO_2 fuel extrusion observed in some of the PCM in-pile experiments[5-8].

4. APPLICATION OF THE MODEL TO IN-PILE TESTS

Extrusion of molten fuel from the center of the fuel pellets into the fuel-cladding gap through radially open cracks in the outer, unmelted region of the pellets has been observed in some of the PCM in-pile experiments[5-8]. In those tests, central fuel melting of up to 80% of the pellet radius was induced in the film boiling zones in which the peak power was ~65 kW/m. In one of those experiments, the extruded fuel failed, in some parts, to reach the fuel-cladding gap (Figure 10). Appreciable extrusion of molten fuel into the fuel-cladding gap was observed, however, in other cases (Figure 11). In this subsection the analytical model development in the previous subsection is applied to assess the differential pressure behind the extruded molten UO_2, the temperature in the molten fuel, T_b, and the subfreezing temperature, $(T_f\text{-}T_w)$, in the solid portion of the fuel pellet in those tests. The crack characteristics used in the calculations were measured from Figure 10, and are as follows: $a_i = 3.75 \times 10^{-5}$ m; $a_e = 4 \times 10^{-4}$ m; and $L = 2.4 \times 10^{-3}$ m.

The thermophysical properties for solid and molten UO_2 used in the calculations are

Fuel melting point (K)	3100
Density of molten fuel (10^3 kg/m^3)	8.74
Density of solid fuel (10^3 kg/m^3)	9.70
Heat capacity of solid fuel (J/kg·K)	394
Thermal conductivity of molten fuel (W/m·k)	2.50
Thermal conductivity of solid fuel (W/m·k)	2.53
Viscosity of molten fuel (10^{-2} poises)	4.24
Latent heat of fusion (J/kg)	2.74×10^5

Figure 20 shows the molten fuel maximum penetration length in the crack, versus the driving pressure difference between the center of the pellet and the fuel-cladding gap for different subfreezing temperatures in the crack walls, $(T_f\text{-}T_w)$. In the results presented in Figure 20, the molten fuel is at the melting point. As indicated, penetration of molten fuel into pellet radial cracks depends on both the subfreezing in the crack walls and the differential pressure across the crack. Increasing the differential pressure or decreasing the subfreezing temperature (that is, slower growth rate of the crust at the crack entrance) increases the penetration length of the fuel before the crack entrance is completely blocked. Note that the capillary forces, P_c,[a] could have played an important part in the radial extrusion process of molten fuel for the cases in which the subfreezing temperature at the crack entrance is less than 20 K. As indicated, the driving pressure required to produce molten fuel relocation in the fuel-cladding gap depends on the subfreezing in the crack walls. When the temperature in the extruded molten fuel is in excess of its melting point, the growing solidified crust reaches a steady state thickness which is less than half the width of the crack opening, a_j, as shown in Figure 21. In this case, molten fuel continues to flow from the center of the pellet and relocate in the fuel gap since only partial blockage of the crack is obtainable. Increasing the temperature of molten fuel [that is, increasing $(T_b - T_f)$] or decreasing the subfreezing temperature in the steady state crack wall (that is, $T_f - T_w$), decreases the maximum thickness obtainable for the crust at the crack entrance, allowing more molten UO_2 to flow through the crack and relocate in the fuel-cladding gap.

The results of such an applied study indicate that the superheating in the extruded molten UO_2 and the pressure at the pellet center play a significant role in determining whether or not the molten fuel at the pellet center can relocate in the fuel-cladding gap prior to complete blockage of the crack by solidification of molten fuel on the crack wall. The failure of molten UO_2, in some of the in-pile tests, to completely penetrate the radial crack and relocate in the fuel-cladding gap (Figure 10) was due to the fact that the extruded molten fuel was at its melting point and the driving pressure was very small (that is, less than 0.004 MPa), which induced an early blockage of the crack (as explained in the previous paragraph). The temperature in the solid fuel at the crack entrance, however, should have been close to the UO_2 melting point (that is, small subfreezing). The driving pressure, in this case, might have been induced by the capillary forces because of the small width of the crack in the unmelted periphery of the fuel pellet. In the other cases, in which appreciable extrusion of molten fuel was observed in the fuel-cladding gap, the molten fuel must have been slightly superheated, so that complete crack blockage due to freezing was not obtainable and molten fuel continued to flow from the central melting zone into the fuel-cladding gap.

---

a. The capillary pressure, P_c, is evaluated from the relation[24], $P_c \cong 2\Upsilon/a_j\,(1 + \Upsilon/2)$, where Υ is the surface energy of molten UO_2 in the neighborhood of the melting point. A value of 0.45 N/m was recommended[39] for Υ.

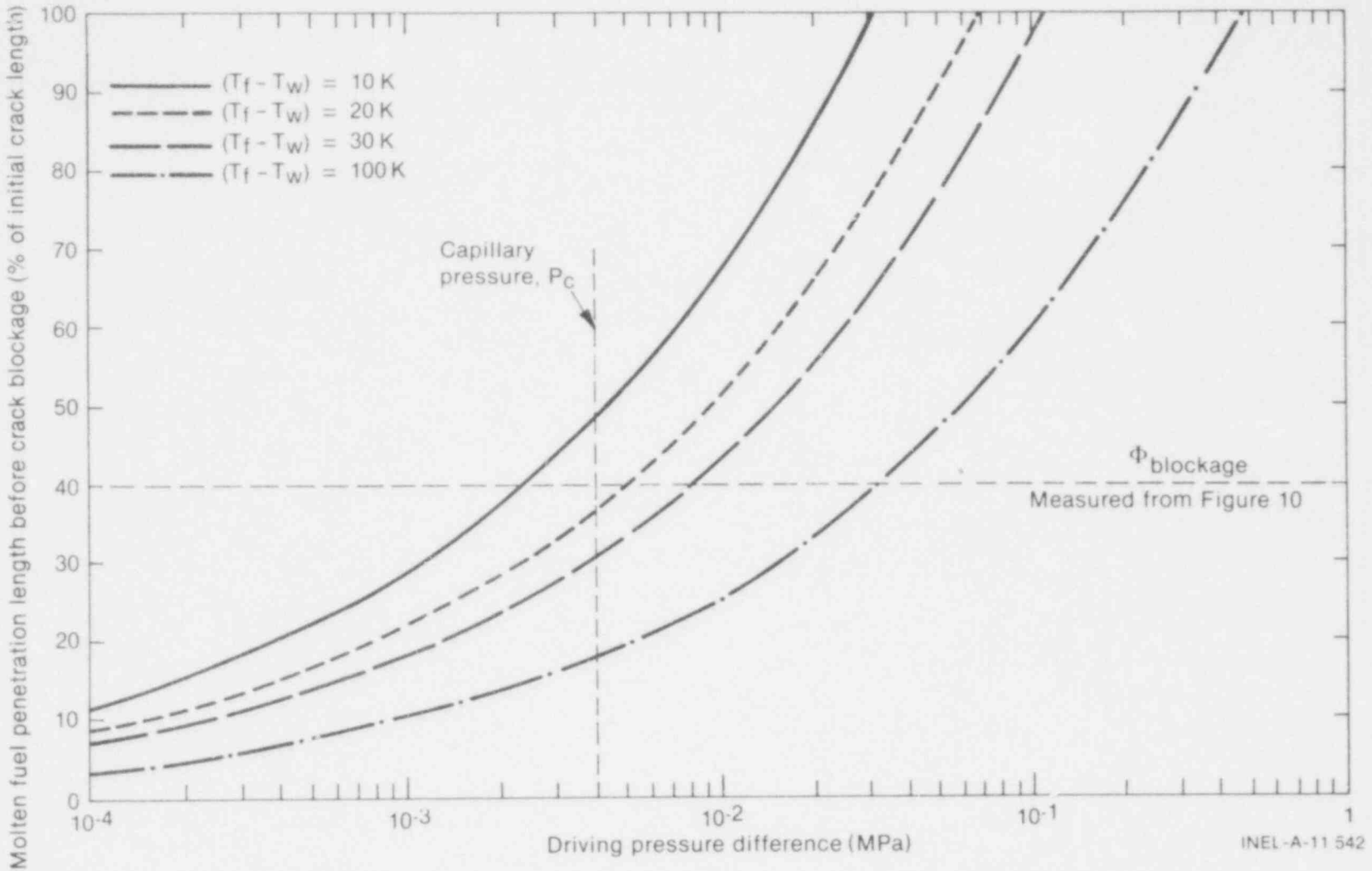

Fig. 20 UO_2 fuel maximum penetration length as a function of driving pressure and subf eezing in crack walls.

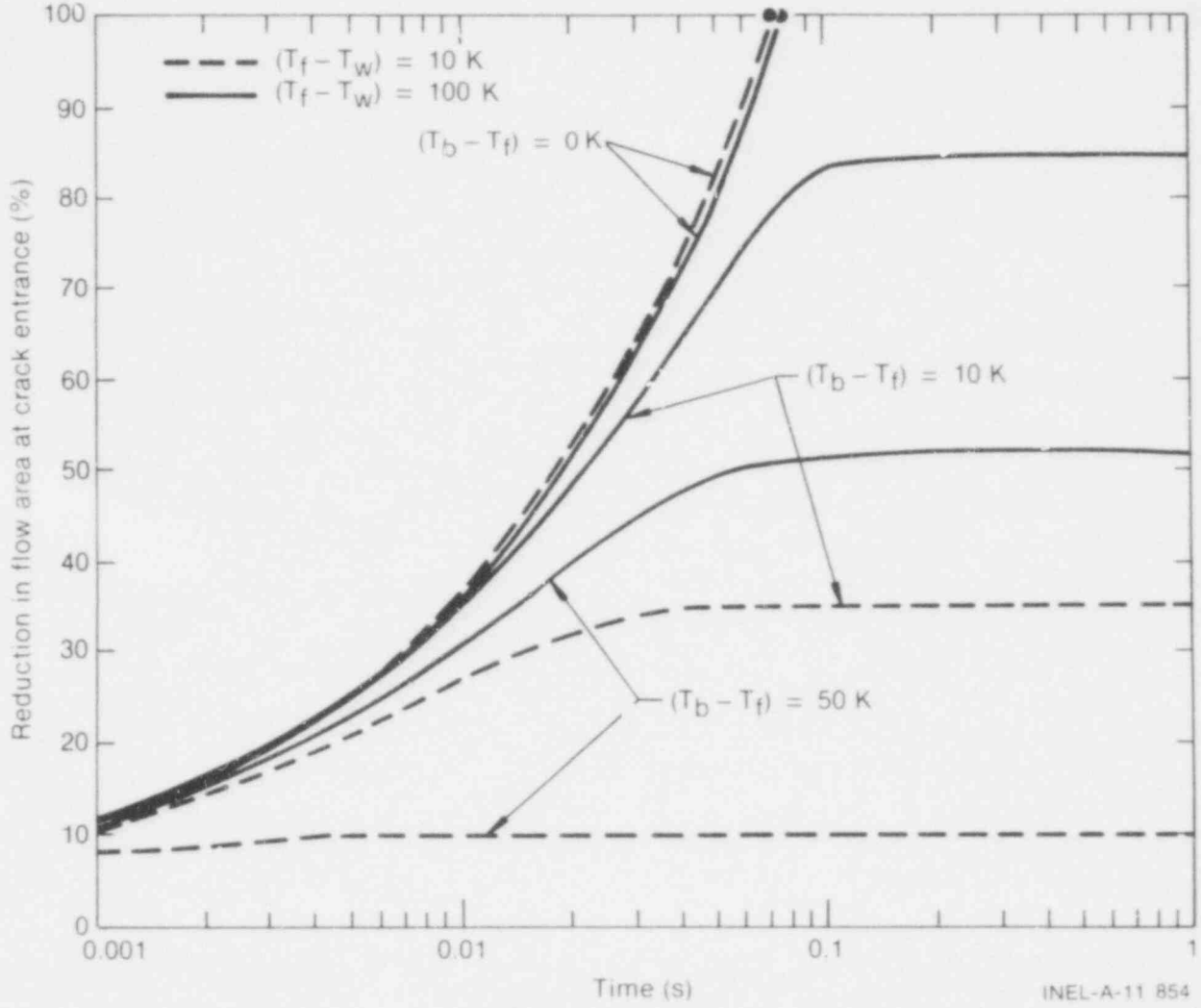

Fig. 21 Reduction in flow area at the crack entrance as a function of time and superheating in the extruded molten fuel.

IV. CONDITIONS FOR UO_2 FUEL FREEZING AND ZIRCALOY CLADDING SIMULTANEOUS MELTING UPON CONTACT

Conditions under which molten UO_2 may extrude into radial cracks in the pellet and relocate into the fuel-cladding gap were evaluated in the preceding section. If the amount of extruded molten fuel is sufficient to fill the fuel-cladding gap in a local area, physical contact between the molten UO_2 and zircaloy cladding will occur, and melting of the zircaloy cladding could begin at its inside surface. The purpose of this section is to determine the conditions for fuel freezing and the potential for simultaneous melting of the zircaloy cladding upon contact, and thereby evaluate the circumstances under which cladding melting due to contact with molten UO_2 is possible. The exact analytical solution for the transient temperature field and the progress of solidification and melting fronts in the neighborhood of an interface separating initially molten and solid regions at different uniform temperatures has been introduced by Epstein[40]. The physical model is illustrated in Figure 22. The conditions for molten UO_2 fuel freezing and the potential for simultaneous melting of the zircaloy cladding upon contact are obtained by simultaneously solving the following transcendental equations[40]:

$$\operatorname{erf}(\lambda) = \frac{1}{\sigma\,\theta_2} \tag{32}$$

and

$$\frac{\sigma\theta_2}{\exp(\lambda^2)} - \frac{\theta_1}{\exp(\beta_{sm}^2\,\lambda^2)\,\operatorname{erfc}(\beta_{sm}\lambda)} = \frac{\lambda\sqrt{\pi}}{SN} \tag{33}$$

where

λ = freezing constant of molten fuel

$$\sigma = \left(k_{inc}\,\rho_{mc}\,C_{p_{inc}}/k_{sf}\,\rho_{sf}\,C_{p_{sf}}\right)^{1/2}$$

$$\theta_1 = \left(k_{mf}\,\rho_{mf}\,C_{p_{mf}}/k_{sf}\,\rho_{sf}\,C_{p_{sf}}\right)^{1/2}\left(\frac{T_b - T_f}{T_f - T_{mp}}\right)$$

$$\theta_2 = \left(k_{sc}\,\rho_{sc}\,C_{p_{sc}}/k_{mc}\,\rho_{mc}\,C_{p_{mc}}\right)^{1/2}\left(\frac{T_{mp} - T_o}{T_f - T_{mp}}\right)$$

$$\beta_{sm} = (\alpha_{sf}/\alpha_{mf})^{1/2}$$

$$SN = C_{p_{sf}}(T_f - T_{mp})/h_f.$$

In this analysis, constant but different thermophysical properties for the solid and liquid phases in the fuel and the cladding regions are considered. Also, a good wetting characteristic between molten UO_2 and

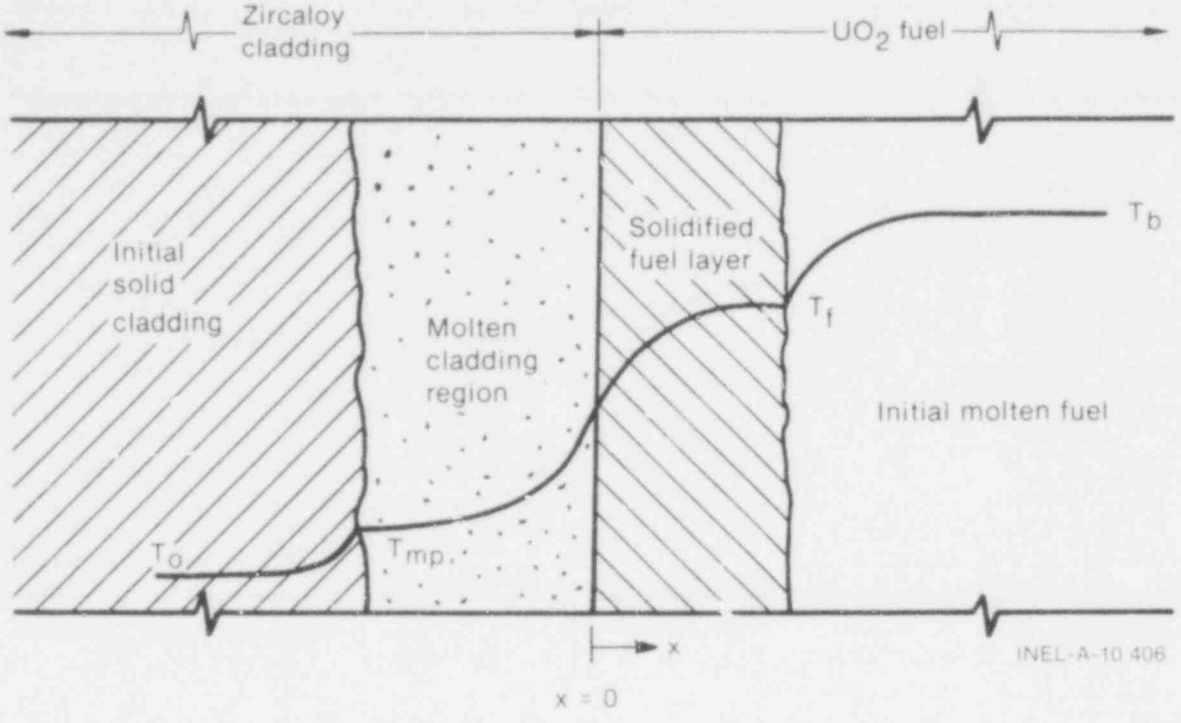

Fig. 22 Physical model for the freezing of stagnant molten fuel on simultaneously melting zircaloy cladding.

zircaloy cladding is assumed. This assumption[23] is reasonable and can be understood through consideration of Young's equation

$$\gamma_{LV} \cos \theta = \gamma_{SV} - \gamma_{SL} \tag{34}$$

which relates θ(the contact angle) to the liquid surface tension, γ_{LV}, the solid surface tension, γ_{SV}, and the solid-liquid interfacial tension, γ_{SL}, as demonstrated in Figure 23. It is convenient in practical application to consider the ratio

$$w = \left(\frac{\gamma_{SV} - \gamma_{SL}}{\gamma_{LV}} \right) \tag{35}$$

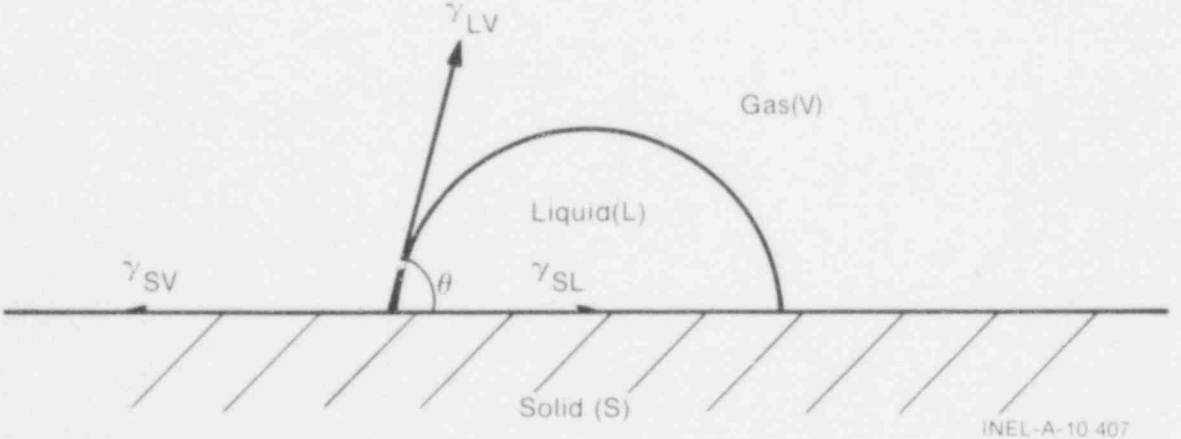

Fig. 23 Illustration of a sessile drop, indicating the contact angle at the surface and the interfacial forces.

491 049

where w is equal to the cosine of the contact angle; w may be called the wetting coefficient. If $w \geq 1$, the solid is completely wetted by the liquid, whereas if $w \leq -1$, the solid is not wetted. When $-1 < w < 1$, the solid is partially wetted.

The chemical reduction of molten UO_2 at the interface of contact with the zircaloy cladding results in a considerable decrease in γ_{SL} from the large value associated with chemically dissimilar materials (ceramic-metal), to a smaller value associated with chemically similar material (metal-metal or oxide-oxide). This reduction in γ_{SL} causes a precipitous decrease of θ (that is, complete wetting where w could be greater than or equal to unity).

The thermophysical properties for zircaloy cladding used in the analysis are listed in Table III. Figure 24 illustrates an initial temperature map for the UO_2-zircaloy system. The value of the interface temperature between molten fuel and zircaloy cladding depends on the metallurgical characteristics of the cladding at its inside surface (either alpha-zircaloy or ZrO_2). Appendix B presents an assessment of the formation potentials of ZrO_2 on the inside surface of the zircaloy cladding during normal reactor operation. Increasing either the superheat in the extruded molten fuel or the initial temperature of the cladding, so that the combined values are above the curves for either oxygen-stabilized alpha-zircaloy or ZrO_2 in Figure 24, initiates cladding melting and simultaneous fuel freezing, which may eventually result in cladding thermal failure due to partial or complete melting. As indicated in Figure 24, melting of the cladding begins upon being contacted by molten fuel at the fusion temperature, when the initial temperature of the oxygen-stabilized alpha- zircaloy cladding is ≥1660 K. If a layer of ZrO_2 exists at the inside surface of the cladding, the onset of cladding melting at the inside surface (the ZrO_2) would be delayed up to an initial cladding temperature of ~2640 K. At this temperature, the inner layer of the cladding, which may have been in the form of alpha-zircaloy or beta-zircaloy, or both, would already be in a molten state.

TABLE III

THERMOPHYSICAL PROPERTIES OF ZIRCALOY CLADDING

Properties	Alpha-Zircaloy	Beta-Zircaloy	ZrO_2	Reference
Density (10^3 kg/m^3)	6.49	6.44	5.82	(41)
Specific heat (J/kg·K)	375	650	604.8 (42)	(16)
Thermal conductivity (W/m·K)	19.6	28.5	2.2	(16)
Latent heat of fusion (J/kg)	2.25×10^5	2.25×10^5	7.06×10^5 (42)	(16)
Melting point (K)	2245.0	2125.0	2950.0	(16)
Boiling point (K)	--	3853.0	4548.0	(43)

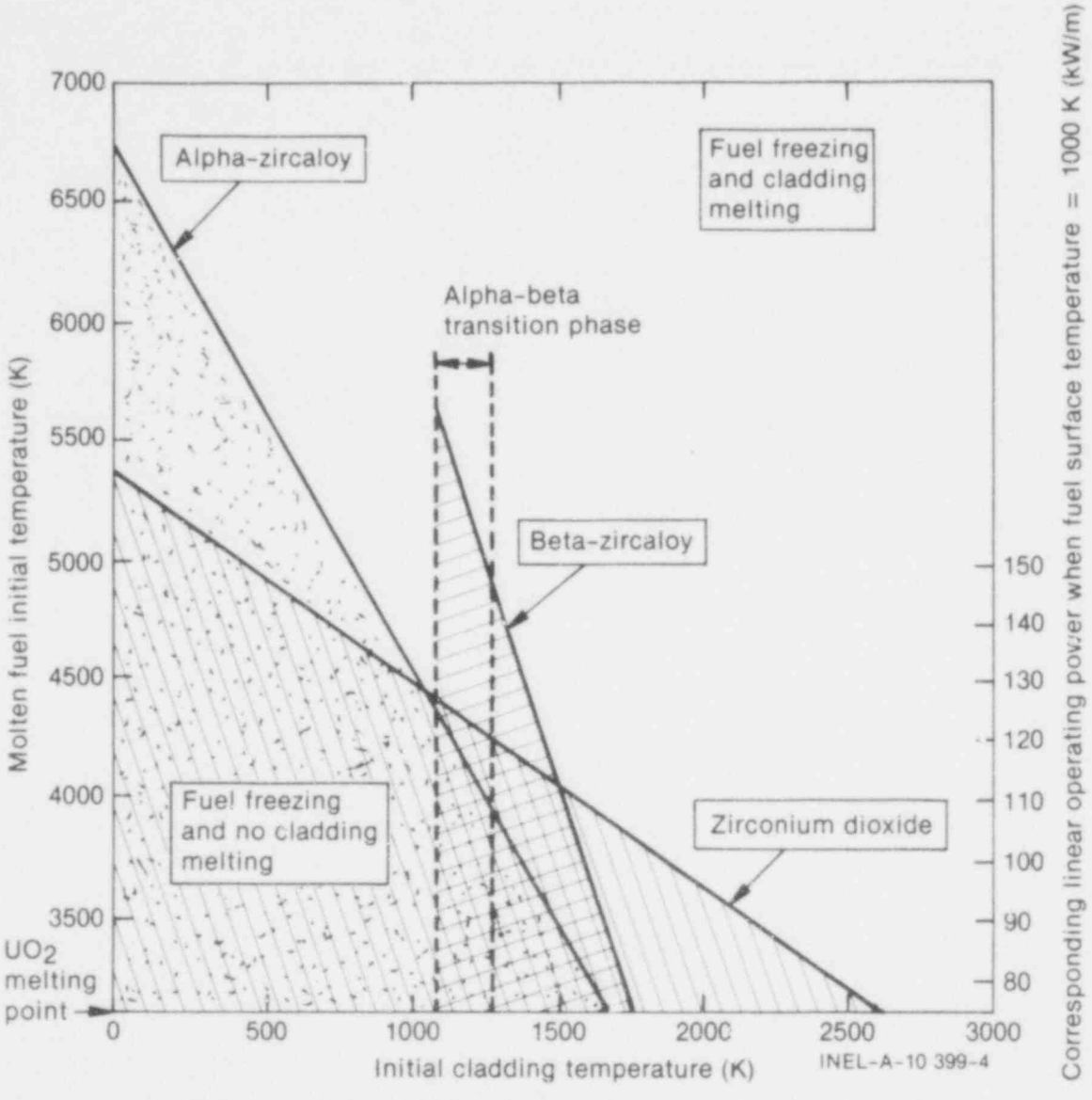

Fig. 24 Temperature map for initially molten UO_2 contacting initially solid zircaloy cladding.

491 051

The results presented in Figure 24 for the conditions of molten UO_2 freezing and zircaloy cladding simultaneous melting upon contact are consistent with the experimental observations from the in-pile tests[5-8] in which an extensive amount of molten fuel was extruded from the central zone into the fuel- cladding gap without producing any cladding melting (for example, Figure 11). In those tests, the cladding temperature (as evaluated from the postirradiation examinations by measuring the ZrO_2 layer produced during film boiling on the outer surface of the cladding) was sufficiently low, so that when molten fuel contacted the zircaloy cladding, simultaneous cladding melting did not occur. Table IV presents a comparison of the experimental observations from the postirradiation examinations of the in-pile tests with the analytical data from Figure 24. This comparison is based on the estimated maximum cladding temperature during film boiling[4] and the experimental finding of the metallurgical characteristics at the inside surface of the zircaloy cladding[5-8] (either oxygen-stabilized alpha-zircaloy or ZrO_2). In this comparison, the extruded molten fuel is considered to be at its fusion temperature. As shown in Table IV, the analytical predictions are consistent with the results from the in-pile experiments.

COMPARISON OF EXPERIMENTAL OBSERVATIONS
THEORETICAL PREDICTIONS FOR THE POTENTIAL FOR ZIR

Test	Rod	Average Burnup (MWd/t)	Fuel Stack Length (m)	Filling Pressure (MPa)		Rod P... Durin... Film Boiling (kW/m)		Isothe... Effect... Claddi... Tempera... Durin... Film Bo... (K) (best est...
				At Assembly	Prior to Test	Peak	Local	
IE-1	IE-009	16 640	0.89	2.61	1.91	63.7	53	127
IE-3	IE-015	11 060	0.97	2.56	2.36	69	59.03	175
IE-3	IE-016	8850	0.97	2.65	2.46	69	50.03	188

TABLE IV

FROM THE IRRADIATION EFFECTS TEST SERIES[5-8] WITH
CALOY CLADDING MELTING UPON BEING CONTACTED BY MOLTEN FUEL

rmal ive ng ture g iling imate)[a]	Exposure Time in Film Boiling (s)	Location of Local Power from the Bottom of the Rod (m)	Postirradiation Examination Results	Theoretical Predictions from Figure 24	Observations[5-8]
0	60	0.579 to 0.597	Pellet cracking, central fuel melting with molten fuel extrusion to the cladding surface, cladding collapse with no evidence of prior cladding melting. A 24-μm-thick oxygen stabilized α-zircaloy layer has been formed at the inside cladding surface.	No cladding melting	No cladding melting
0	84	0.660 to 0.679	Central fuel melting, once-molten fuel extrusion through radially open cracks. The solidification of molten fuel on the crack walls caused the blockage of such cracks before enough molten fuel could be extruded to fill the fuel-cladding gap. Formation of a 15-μm-thick ZrO_2 layer that was at the cladding inside surface[b].	No cladding melting	No cladding melting
0	47	0.718	Central fuel melting, once-molten fuel extrusion through pellet dishes and into the fuel-cladding gap. The formation of a 10-μm-thick ZrO_2 layer on the inside cladding surface. Zircaloy cladding collapse onto the fuel.	No cladding melting	No cladding melting

V. DISCUSSION AND CONCLUSIONS

Fuel conditions during a power-cooling-mismatch event in light water reactors have been reviewed and characterized with regard to pellet cracking, fuel melting, and molten fuel radial extrusion. During normal operation of the reactor, fuel cracking usually occurs along radial and horizontal planes at the periphery of the pellet in which the induced thermoelastic strain exceeds the UO_2 fuel tensile strength. Crack size and population depend on the reactor power and the irradiation history of the fuel.

If a PCM accident occurs in an LWR, film boiling may begin at the outer surface of the cladding, causing a rapid increase in the fuel and cladding temperatures. Fuel melting can start at the pellet centerline, propagating radially outward. Volumetric expansion at the pellet center due to fuel melting, fission gas release within the melting zone, and fuel vapor pressure increase the crack openings at the outer, unmelted portion of the pellet and act as driving forces to cause molten fuel extrusion through the radially open cracks into the fuel-cladding gap.

The transient freezing and penetration of a superheated liquid through a short, initially empty crack maintained at a constant, uniform temperature is modeled and studied analytically. A parametric analysis is presented illustrating that the process of liquid penetration into an initially empty crack depends mainly on the driving pressure across the crack, the crack length, and the crack shape (that is, a divergent, a parallel wall, or a convergent crack). However, the simultaneous growth of the deposited crust on the crack walls is mainly governed by the subfreezing in the wall and the superheating in the penetrating liquid. For a liquid at its fusion temperature, the frozen crust continues to grow with time until it eventually produces complete blockage of the crack. When the liquid is superheated, however, the growing crust approaches a steady state thickness which might be less than the half width of the crack opening. In the latter case, complete blockage of the crack is impossible; only partial blockage would occur.

Application of the freezing and penetration analysis to molten fuel extrusion observed in the PCM in-pile tests indicates that the molten fuel superheating and the pressure at the pellet center have played a significant role in determining whether or not molten fuel would relocate into the fuel-cladding gap before crack blockage occurs because of the solidification of molten fuel on the crack walls. For molten fuel at the center of the pellet to relocate into the fuel-cladding gap, the fuel must be superheated so that the deposited frozen crust on the crack walls continues to grow until it reaches a steady state thickness less than half the width of the crack, and thus produces only partial crack blockage. Otherwise, crack blockage would occur before the extruded molten fuel could completely penetrate the crack. The driving pressure at the pellet center in those in-pile tests could have been due to capillary forces (~0.004 MPa), because of the small width of the cracks (~75 μm), if the subfreezing in the crack walls was less than 20 K. Although the fuel vapor pressure can be much higher, since molten fuel superheating at the pellet center may reach several hundred degrees (for example, 0.1 MPa when fuel superheating is ~500 K), the axial movement of molten fuel could have been a cause for reducing the pressure at the pellet center.

Conditions for potential melting of the zircaloy cladding upon being contacted by the extruded molten UO_2 were assessed, using an exact analytical model for the freezing of a stagnant superheated liquid on a semi-infinite, initially solid wall undergoing simultaneous melting. The onset of cladding melting at its inner surface upon being contacted by molten UO_2 is governed by two parameters: (a) the metallurgical composition at the inner surface of the cladding (that is, alpha-zircaloy or ZrO_2), and (b) the temperatures of the molten fuel and the cladding at the time of contact. Melting at the inner surface of the oxygen-stabilized alpha-zircaloy cladding upon being contacted by molten UO_2 at its fusion temperature would begin when the cladding temperature is greater than 1660 K. If a layer of ZrO_2 forms at the inner surface of the cladding, cladding melting (the ZrO_2) would begin at cladding temperatures greater than ~2640 K. At this temperature, the middle layers of the cladding (which may have been either oxygen- stabilized alpha-zircaloy or beta-zircaloy, or both) would already be in a molten state. If the extruded molten fuel is superheated, however, cladding melting would start at the fuel-cladding interface at progressively lower cladding temperatures.

In the PCM in-pile tests, a ZrO_2 or an oxygen-stabilized alpha-zircaloy layer was formed at the inner surface of the cladding. Melting of the cladding which was in contact with the extruded molten fuel was not observed when either layer was present (Table IV). The absence of cladding melting was concluded to be due to the fact that molten fuel and zircaloy-cladding temperatures were below the level required to initiate fuel freezing and simultaneous cladding melting upon contact.

VI. REFERENCES

1. R. C. Ballinger, W. G. Dobson, R. R. Biederman, "Oxidation Reaction Kinetics of Zircaloy-4 in an Unlimited Steam Environment," *Journal of Nuclear Materials, 62* (1976) pp 213-270.

2. A. W. Cronenberg and M. S. El-Genk, "An Assessment of Oxygen Diffusion During UO_2-Zircaloy Interaction," *Journal of Nuclear Materials, 78* (1978) pp 390-407.

3. A. W. Cronenberg and M. S. El-Genk, "A Comparison of Cladding Microstructure Resulting from UO_2-Zircaloy Interaction with a Diffusional Assessment of Oxygen Transport for a Coupled Two-Media Problem," *4th International Conference on Zirconium in the Nuclear Industry, Stratford-on-Avon, England, June 26-29, 1978.*

4. S. L. Seiffert and R. R. Hobbins, *Oxidation and Embrittlement of Zircaloy-4 Cladding from High Temperature Film Boiling Operation*, NUREG/CR-0517, TREE-1327 (April 1979).

5. A. S. Mehner and R. S. Semken, *Postirradiation Examination Results for the Irradiation Effects Test IE-1*, TREE-NUREG-1199 (February 1978).

6. S. A. Ploger and T. F. Cook, *Postirradiation Examination Results for the Irradiation Effects Test IE-3*, TREE-NUREG-1200 (March 1978).

7. T. F. Cook, S. A. Ploger, R. R. Hobbins, *Postirradiation Examination Results for the Irradiation Effects Test IE-5*, TREE-NUREG-1201 (March 1978).

8. A. S. Mehner et al, "Performance of Unirradiated and Irradiated PWR Fuel Rods Tested Under Power-Cooling-Mismatch Conditions," *Thermal Reactor Safety Meeting, Sun Valley, Idaho, July 31 - August 5, 1977.*

9. A. G. Evans and R. W. Davidge, "The Strength and Fracture of Stoichiometric Polycrystalline UO_2," *Journal of Nuclear Materials, 33* (1969) pp 249-260.

10. R. F. Canon, J. T. A. Roberts, R. J. Beals, "Deformation of UO_2 at High Temperatures," *Journal of the American Ceramic Society, 54* (1971) pp 105-112.

11. J. T. A. Roberts and Y. Ueda, "Influence of Porosity on Deformation and Fracture of UO_2," *Journal of the American Ceramic Society, 55* (1972) pp 117-124.

12.[a] G. H. Chalder, "Zircaloy-Clad UO_2; A Review of Properties and Performance," *Enlarged Halden Programme Groups Meeting on Computer Control and Fuel Research Related to Safe and Economic Plant Operation*, HDR 188 (1974).

13. J. Veeder, *Thermo-Elastic Expansion of Finite Cylinders*, AECL-2660 (1967).

14.[a] M. Ichikawa, "Analysis of Fuel Deformation by the Finite Element Method," *Enlarged Halden Programme Groups Meeting on Computer Control and Fuel Research Related to Safe and Economic Plant Operation*, HDR 188 (1974).

15. B. A. Murdock, *Gap Conductance Test Series, Test GC 1-3 Postirradiation Examination*, TREE-NUREG-1088 (1977).

---

a. Halden project use only.

16. P. F MacDonald and L. B. Thompson (eds), *MATPRO - Version 09, A Handbook of Material Properties for Use in the Analysis of Light Water Reactor Fuel Rod Behavior*, TREE-NUREG-1005 (December 1976).

17. J. A. Christensen, "Thermal Expansion and Change in Volume of Uranium Dioxide on Melting," *Journal of the American Ceramic Society, 46* (1963) p 607.

18. R. E. Woodley, "The Viscosity of Molten Uranium Dioxide," *Journal of Nuclear Materials, 50* (1974) pp 103-106.

19. B. F. Rubin, *Summary of (U, Pu) O_2 Properties and Fabrication Methods*, GEAP-13582 (1970).

20. I. Catton and R. C. Erdmann, *Post-Accident Core Retention for LMFBRs*, UCLA-ENG-7343 (1973).

21. D. W. Croucher et al, *Irradiation Effects Test Series, Test IE-5 Test Results Report*, TREE-NUREG-1130 (1978).

22. D. T. Livey and P. Murray, "The Wetting of Solid Oxides and Carbides by Liquid Metals," *Sintered High-Temperature and Corrosion-Resistant Materials, 2nd Plansee-Seminar, June 19-23, 1955*, pp 375-405.

23. J. G. Eberhart, *The Wettability of Reactor Fuel by Molten Metal*, ANL-RDP-22 (November 1973) pp 7.26-7.27.

24. J. J. Bikerman, *Physical Surfaces*, New York and London: Academic Press, 1970.

25. R. W. Ohse et al, "Extension of Vapor Pressure Measurements of Nuclear Fuels (U, Pu) O_2 and UO_2 to 7000 K for Fast Reactor Safety Analysis," *Journal of Nuclear Materials, 59* (1976) pp 112-124.

26. E. A. Fisher et al, "Critical Assessment of Equation of State Data for UO_2," *Journal of Nuclear Materials, 59* (1976) pp 125-136.

27. D. C. Menzies, *The Equation of State of Uranium Dioxide at High Temperatures and Pressures*, TRG Report 1119 (D) (1966).

28. P. A. Finn et al, "Equation of State of Uranium Dioxide," *Journal of Nuclear Materials, 79* (1979) pp 14-19.

29. M. Epstein et al, "Transient Freezing of a Flowing Ceramic Fuel in a Steel Channel," *Nuclear Science and Engineering, 61* (1976) pp 310-313.

30. F. B. Cheung and L. Baker, Jr., "Transient Freezing of Liquids in Tube Flow," *Nuclear Science and Engineering, 60* (1976) pp 1-9.

31. M. Epstein, A. Yim, F. B. Cheung, "Freezing Controlled Penetration of a Saturated Liquid into a Cold Tube," *Journal of Heat Transfer, 99* (1977) pp 233-238.

32. M. Epstein and G. M. Hauser, "Solidification of a Liquid Penetrating into a Convectively Cooled Tube," *Letters in Heat and Mass Transfer, 5* (1978) pp 19-28.

33. K. Stephan, "Influence of Heat Transfer on Melting and Solidification in Forced Flow," *International Journal of Heat Mass Transfer, 12* (1969) pp 199-213.

34. J. Madejski, "Solidification in Flow Through Channels and into Cavities," *International Journal of Heat Mass Transfer, 19* (1976) pp 1351-1356.

35. M. Epstein and G. M. Hauser, "Freezing of an Advanced Tube Flow," *Journal of Heat Transfer, 99* (1977) pp 687-689.

36. W. M. Rottsenow and J. P. Hartnett, *Handbook of Heat Transfer*, New York: McGraw-Hill, Inc., 1973.

37. P. M. Heertjes and Ir. Ong Tjing Gie, "Crystalization of Water of Unidirectional Cooling," *British Chemical Engineering, 5* (1960) pp 413-419.

38. H. S. Carslaw and J. C. Jaeger, *Conduction of Heat in Solids*, (2nd ed) London: Oxford University Press, 1959.

39. M. G. Chasanov, L. Leibowitz, S. D. Gabelnick, "High Temperature Physical Properties of Fast Reactor Materials," *Journal of Nuclear Materials, 49* (1973/74) pp 129-135.

40. M. Epstein, "Heat Conduction in the UO_2 Cladding Composite Body with Simultaneous Solidification and Melting," *Journal of Nuclear Science and Engineering, 51* (1973) pp 84-87.

41. M. O. Tucker, A. F. Brown, T. Healey, "Partitioning of Oxygen in Steam Oxidized Zircaloy," *Proceedings of Specialists Meeting on the Behavior of Water Reactor Fuel Elements Under Accident Conditions, OECD/Nuclear Energy Agency, Norway* (September 1976).

42. T. L. Markm, "Preparation of Nuclear Fuel," *Nuclear Engineering, Part VVIII, 63(80)* (1957) p 43.

43. *JANAF Thermochemical Tables*, NSRDS-NBS 37, National Bureau of Standards, and Supplements (1971).

APPENDIX A

STEADY STATE ANALYSIS OF THE TEMPERATURE DISTRIBUTION IN THE MOLTEN AND SOLID REGIONS OF A CYLINDRICAL FUEL PELLET

APPENDIX A

STEADY STATE ANALYSIS OF THE TEMPERATURE DISTRIBUTION IN THE MOLTEN AND SOLID REGIONS OF A CYLINDRICAL FUEL PELLET

This appendix presents a derivation of the temperature integral in both the molten and the solid regions of a cylindrical fuel pellet. The temperature integrals are used to determine the temperature distribution, molten fuel radius, and the amount of superheating of molten fuel at the center of the pellet.

From the total heat balance in both the solid and molten regions of a cylindrical fuel pellet (Figure A-1 presents a schematic diagram of a cylindrical fuel pellet with central fuel melting) the following is obtained:

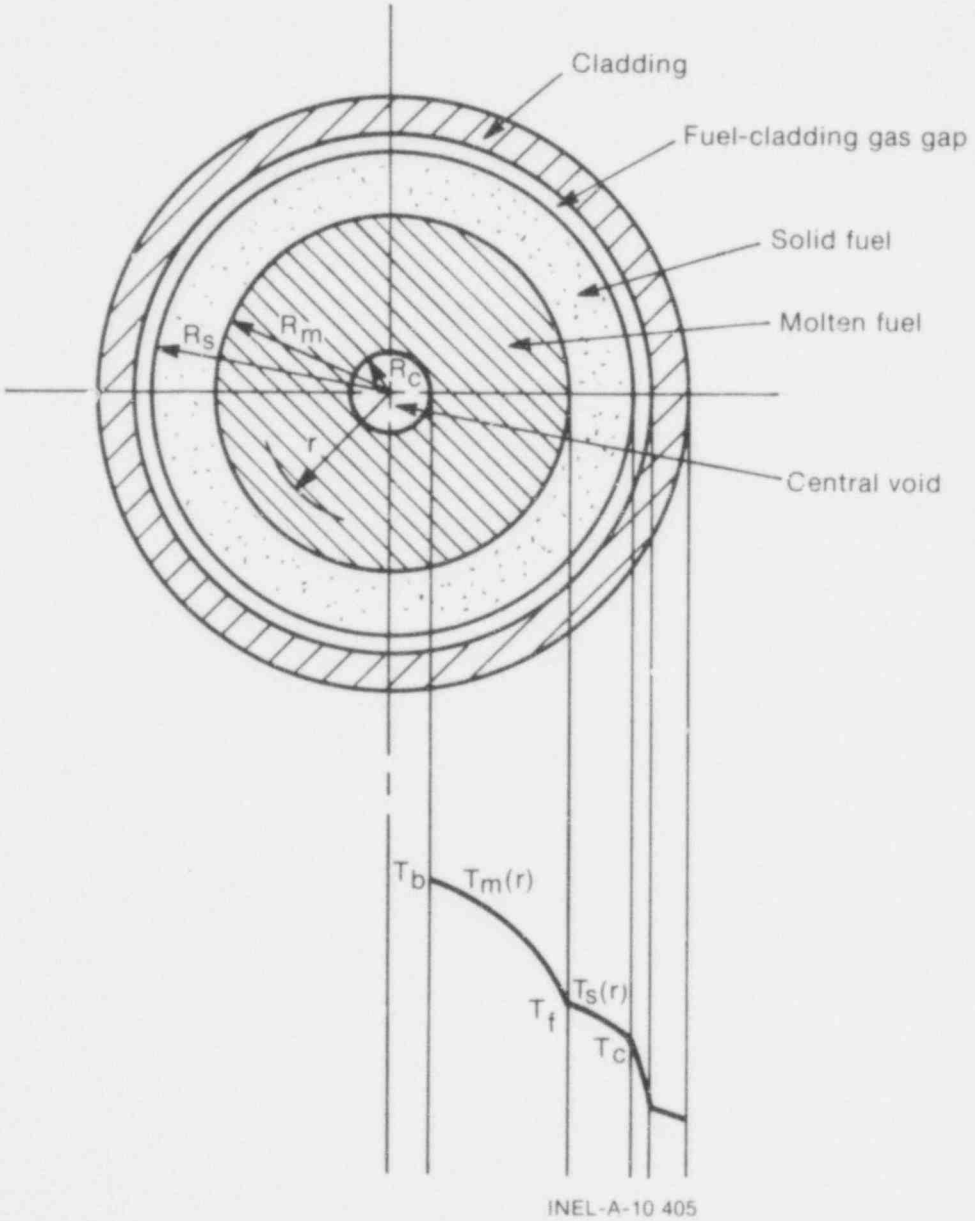

Fig. A-1. Schematic of a cylindrical fuel pellet with central fuel melting.

$$\dot{q} = \pi (R_m^2 - R_c^2) \dddot{q}_m + \pi (R_s^2 - R_m^2) \dddot{q}_s \qquad \text{(A-1)}$$

where

$\dot{q}$ = the operating linear power, kW/m

R_c = the central void radius, m

R_m = the molten fuel radius, m

R_s = the fuel pellet radius, m

$\dddot{q}_m$ = the volumetric heat generation in the molten fuel, kW/m^3

$\dddot{q}_s$ = the volumetric heat generation in the solid fuel, kW/m^3.

Equation (A-1) can be rewritten as

$$\dot{q} = \dddot{q}_s \pi R_s^2 \left\{ d\left[(R_m/R_s)^2 - (R_c/R_s)^2\right] + \left[1 - (R_m/R_s)^2\right] \right\} \qquad \text{(A-2)}$$

where

$\dddot{q}_m = \dddot{q}_s \cdot d$

$d = (\bar{\rho}_m/\bar{\rho}_s)$

$\bar{\rho}_m$ = molten fuel average density

$$= \left(\int_{T_f}^{T_b} \rho_m(T)\, dT \right) \Big/ (T_b - T_f)$$

$\bar{\rho}_s$ = solid fuel average density

$$= \left(\int_{T_c}^{T_f} \rho_s(T)\, dT \right) \Big/ (T_f - T_c)$$

T_b = temperature of molten fuel, K

T_c = temperature at the surface of the fuel pellet, K

T_f = fusion temperature, K.

Steady state heat conduction in both the molten and solid regions of the fuel pellet is described by the set of equations and boundary conditions listed in Table A-I. The integration of the heat conduction equation in the molten fuel region, $R_c \le r \le R_m$, once with respect to space from $r = R_c$ to r yields

TABLE A-I

STEADY STATE HEAT CONDUCTION EQUATIONS AND BOUNDARY CONDITIONS IN BOTH THE MOLTEN AND SOLID REGIONS OF A CYLINDRICAL FUEL PELLET

Data	Region	
	Molten Fuel	Solid Fuel
Steady state heat conduction equation	$\frac{1}{r}\frac{\partial}{\partial r}\left(r\,k_m\,\frac{\partial T_m}{\partial r}\right) + q'''_m = 0$	$\frac{1}{r}\frac{\partial}{\partial r}\left(r\,k_s\,\frac{\partial T_s}{\partial r}\right) + q'''_s = 0$
Boundary conditions	$T_m\,(R_m) = T_f$	$T_s\,(R_m) = T_f$
	$k_m\,\frac{\partial T_m}{\partial r}\,(R_c) = 0$	$T_s\,(R_s) = T_c$
		$k_s\,\frac{\partial T_s}{\partial r}\,(R_m) = k_m\,\frac{\partial T_m}{\partial r}\,(R_m)$

$$k_m\,\frac{\partial T_m}{\partial r} = \frac{-q'''_m}{2}\left(r - \frac{R_c^2}{r}\right), \tag{A-3}$$

where k_m is the molten fuel thermal conductivity, W/m·K; T_m is the temperature in the molten fuel region of the pellet; and r is a radial coordinate

The reintegration of Equation (A-3) with respect to space from $r = R_c$ to $r = R_m$ yields

$$\int_{T_f}^{T_b} k_m\,dT_m = \frac{-q'''_s d}{4}\,R_s^2\left[(R_m/R_s)^2-(R_c/R_s)^2-2(R_c/R_s)^2\,\ln\,(R_m/R_c)\right]. \tag{A-4}$$

Similarly, the integration of the heat equation in the solid fuel region, $R_m \le r \le R_s$, once with respect to space from $r = R_m$ to r results in

$$k_s\,\frac{\partial T_s}{\partial r} = \left(\frac{R_m}{r}\right)\,k_m\,\frac{\partial T_m}{\partial r}\bigg|_{r=R_m} - \frac{q'''_s}{2}\left(r - \frac{R_m^2}{r}\right) \tag{A-5}$$

where k_s is the solid fuel thermal conductivity, W/m·K.

Elimination of the first term on the right side of Equation (A-5) by the aid of Equation (A-3) results in

491 063

$$k_s \left(\frac{\partial T_s}{\partial r}\right) = -\left(\frac{q'''_m}{2r}\right)\left(R_m^2 - R_c^2\right) - \frac{q'''_s}{2}\left(r - \frac{R_m^2}{r}\right). \tag{A-6}$$

Integrating Equation (A-6) once with respect to space from $r = R_m$ to $r = R_s$ yields

$$\int_{T_c}^{T_f} k_s \, dT_s = \left(\frac{q'''_s}{4} R_s^2\right)\left\{1 - (R_m/R_s)^2 + 2(R_m/R_s)^2 \ln (R_m/R_s) - 2d\left[(R_m/R_s)^2 - (R_c/R_s)^2\right] \ln (R_m/R_s)\right\}. \tag{A-7}$$

Eliminating q_s between Equation (A-2) and Equations (A-4) and (A-7), respectively, gives

$$\int_{T_f}^{T_b} k_m \, dT_m = \frac{q'_d}{4\pi}\left\{\frac{(R_m/R_s)^2 - (R_c/R_s)^2 - 2(R_c/R_s)^2 \ln(R_m/R_c)}{d\left[(R_m/R_s)^2 - (R_c/R_s)^2\right] + \left[1 - (R_m/R_s)^2\right]}\right\} \tag{A-8}$$

and

$$\int_{T_c}^{T_f} k_s \, dT_s = \frac{q'}{4\pi}\left\{\frac{\left[1 - (R_m/R_s)^2 + 2(R_m/R_s)^2 \ln (R_m/R_s)\right] - 2d\left[(R_m/R_s)^2 - (R_c/R_s)^2\right] \ln (R_m/R_s)}{d\left[(R_m/R_s)^2 - (R_c/R_s)^2\right] + \left[1 - (R_m/R_s)^2\right]}\right\}. \tag{A-9}$$

Equations (A-8) and (A-9) give the temperature integral in the molten and solid regions of a cylindrical fuel pellet in terms of the molten radius and the gaseous void at the center of the pellet. The temperature distribution, the molten fuel radius, and the amount of superheating in the central molten fuel can be determined through use of these equations.

When dealing with a cylindrical fuel pellet with no central void (that is, $R_c = 0$ and, therefore, $R_c/R_m = 0$), Equations (A-8) and (A-9) simplify to

$$\int_{T_f}^{T_b} k_m \, dT_m = \frac{q'}{4\pi}\left[\frac{(R_m/R_s)^2 d}{1 - (R_m/R_s)^2 (1 - d)}\right] \tag{A-10}$$

and

$$\int_{T_c}^{T_f} k_s \, dT_s =$$

$$\frac{\dot{q}'}{4\pi} \left\{ \frac{\left[1 - (R_m/R_s)^2 + 2 (R_m/R_s)^2 \ln (R_m/R_s)\right] - 2 d (R_m/R_s)^2 \ln (R_m/R_s)}{1 - (R_m/R_s)^2 (1 - d)} \right\} . \quad \text{(A-11)}$$

If the molten and solid fuel have the same average density (that is, $\bar{\rho}_m = \bar{\rho}_s$), then the sum of Equations (A-10) and (A-11) reduces to

$$\int_{T_f}^{T_b} k_m \, dT_m + \int_{T_c}^{T_f} k_s \, dT_s = \frac{\dot{q}'}{4\pi} . \quad \text{(A-12)}$$

Furthermore, for $k_m = k_s$, Equation (A-12) becomes

$$\int_{T_c}^{T_b} k_s \, dT_s = \frac{\dot{q}'}{4\pi} . \quad \text{(A-13)}$$

APPENDIX B

POTENTIAL FOR ZrO_2 FORMATION ON THE INSIDE CLADDING SURFACE

APPENDIX B

POTENTIAL FOR ZrO_2 FORMATION ON THE INSIDE CLADDING SURFACE

During off-normal operating conditions in a light water reactor (LWR), such as a power-cooling-mismatch (PCM) event, local film boiling that initiates at the outer surface of the cladding increases the temperature in both the cladding and the fuel pellets. If the external system pressure exceeds the fuel rod internal pressure and the cladding temperature exceeds 920 K, the zircaloy cladding collapses onto the fuel pellets and a solid fuel-cladding interaction begins. As demonstrated in the present work, fuel melting could also begin during a PCM accident at the pellet center and proceed radially outward. One of the parameters which determines whether or not cladding melting may begin at the inside surface upon being contacted by extruded molten fuel during such an accident is the metallurgical composition at the inner surface of the cladding (that is, either alpha-zircaloy or ZrO_2). The presence of a ZrO_2 layer on the inside cladding surface, acting as a thermal barrier, would delay the onset of cladding melting at the inner surface (the ZrO_2) upon being contacted by molten fuel up to an initial cladding temperature of ~2640 K. The formation potential of a ZrO_2 layer on the inner cladding surface during a PCM event is assessed in this appendix.

The key factor in the interaction of UO_2 fuel (either solid or molten) with zircaloy upon contact is the oxygen potential in the fuel ($\Delta\bar{G}_{O_2} = RT \ln P_{O_2}$)[a]. Figure B-1 illustrates the data for the free energies due to the oxygen potential in hypostoichiometric and slightly hyperstoichiometric urania, and Figure B-2

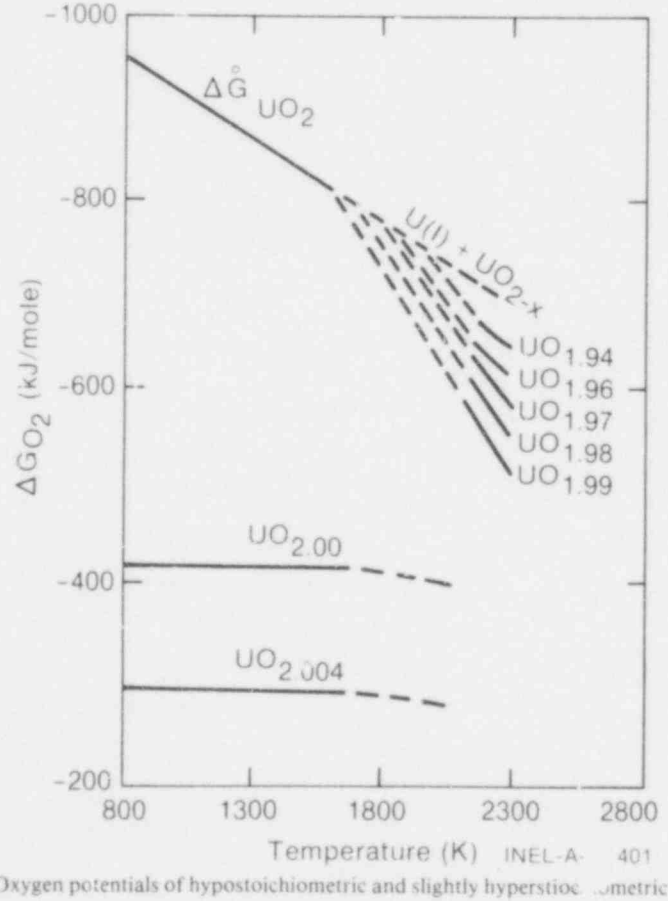

Fig. B-1 Oxygen potentials of hypostoichiometric and slightly hyperstoichiometric urania[B-1].

a. $\Delta\bar{G}_{O_2}$ is the oxygen potential for a stoichiometric urania, R is the universal gas constant, T is the fuel temperature, and P_{O_2} is the oxygen partial pressure in the fuel.

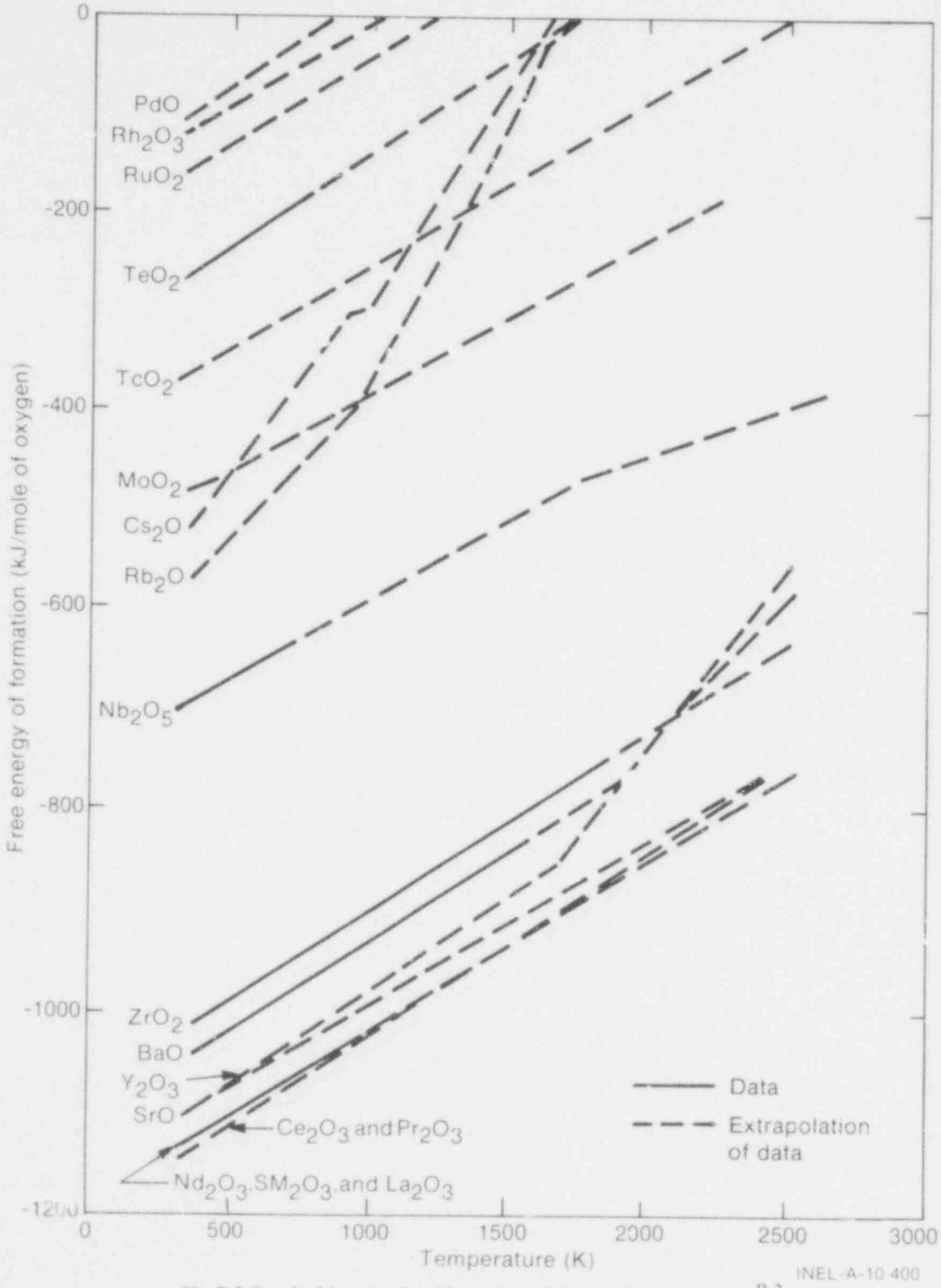

Fig. B-2 Standard free energies of formation of high-yield fission products[B-2].

presents the standard free energies of formation of high-yield fission products. Comparison of the oxygen potential for a stochiometric urania, $(\Delta\bar{G}_{O_2})UO_2$, with the energy of formation for ZrO_2 ($\Delta\mathring{G}_{ZrO_2}$) indicates that

$$(\Delta\bar{G}_{O_2})_{UO_2} > \Delta\mathring{G}_{ZrO_2} \qquad \text{(B-1)}$$

that is, the zircaloy cladding would be expected to oxidize upon being contacted by the molten UO_2 fuel. However, with the presence of an initial oxide layer, the rate of additional oxidation decreases drastically, since oxygen must diffuse through the forming oxide layer. Moreover, the ZrO_2 layer on the inside surface of the cladding may form as a result of oxygen migration across the fuel-cladding gap without physical contact with the UO_2 fuel[B-3].

At cladding temperatures greater than 1400 K, the ZrO_2 layer would be expected to dissolve by the oxygen-stabilized alpha-zircaloy[B-4] transformation. The kinetics of the dissolution depend on the ZrO_2 layer thickness and the time of film boiling during a PCM event. As has been shown from the postirradiation examinations of some fuel rods tested under power-cooling-mismatch conditions in the Power Burst Facility[B-5], a thin layer of ZrO_2 (~10 to 15 μm) was found at the inner surface of the zircaloy cladding in two rods which operated under film boiling conditions for ~47 and 84 seconds, respectively. The cladding temperature in those rods was determined to be about 1880 ± 50 and 1750 ± 50 K, respectively. The undissolved oxide layer at the inside surface of the cladding may have been present because the operating time in film boiling was insufficient to completely dissolve the previously existing ZrO_2 layer by the alpha-zircaloy transformation. (These rods[B-5] were previously irradiated to 8850 and 11 060 MWd/t burnup, respectively.)

REFERENCES

B-1. T. L. Markm, "Preparation of Nuclear Fuel," *Nuclear Engineering, 63* (1967) p 43.

B-2. D. R O'Broyle, F. L. Brown, J. E. Sanecki, "Solid Fission Product Behavior in Uranium-Plutonium Oxide Fuel Irradiated in a Fast Neutron Flux," *Journal of Nuclear Materials, 29* (1969) pp 27-42.

B-3. P. G. Hofmann, Kernforschungszentrum Karlsruhe, West Germany, private communication (1978).

B-4. P. Hofmann and C. Politis, "Chemical Interaction Between UO_2 and Zry-4 in the Temperature Range Between 900 and 1500°C," *4th International Conference on Zirconium in the Nuclear Industry, Stratford-on-Avon, England, June 26-29, 1973.*

B-5. S. A. Ploger and T. F. Cook, *Postirradiation Examination Results for the Irradiation Effects Test IE-3*, TREE-NUREG-1200 (1978).

491 069

DISTRIBUTION RECORD FOR NUREG/CR-0500
(TREE-1270)

Internal Distribution

1 - R. J. Beers, ID

2 - P. E. Litteneker, ID

3-5 - INEL Technical Library

6-7 - Author

8-50 - Special Internal

External Distribution

51-52 - Saul Levine, Director
Office of Nuclear Regulatory Research, NRC
Washington, D.C. 20555

53-58 - Special External

59-355 - Distribution under R3, Water Reactor Safety Research - Fuel Behavior